Finite Element Model Development of the Human Lumbar Spine and Dynamic Stabilization Device Analysis

by

Chaudhry Raza Hassan

A Thesis Submitted to the
Graduate School of Sciences and Engineering
in Partial Fulfillment of the Requirements for
the Degree of

Master of Science
in
Biomedical Sciences & Engineering

Koç University

June 2015

Abstract

Finite element (FE) method is a reliable analysis tool in mechanical engineering as well as in other fields such as electronics and thermodynamics. The use of FE models in biomechanics increased in last couple of decades, particularly in spine biomechanics, largely due to better computational resources available. However, development of spine FE model is a cumbersome and non-trivial task, owing to the complex geometry of the spinal segments. FE models have been used to produce general behaviors of the musculoskeletal systems with almost all physiological and anatomical features.

The main objective of the present thesis is to develop accurate FE models of the human lumbar and thoracic spine. Lumbar FE models are particularly important for the clinicians as well as academicians. It is because low back pain constitute as the most prevalent disease of spine. A novel method was suggested in this thesis to construct an integrated interface between the discs and the vertebrae. The exact geometry was obtained from CT scan data. Multi-block method was used to place nodes over the vertebrae and intervertebral disc surfaces, and hexahedral element was used to mesh the discs and vertebrae. Truss elements were used to simulate the ligaments. Facet joints were simulated by unidirectional gap elements. Material properties were assigned to spinal components using the values from the literature. Pure moments were applied to a flying node which was coupled with top surface of first vertebrae. Lower part of last vertebrae in each model was constrained in all directions. The predicted motion response of FE model was compared with the published in vitro studies in all motion planes and found to be in good agreement.

The validated FE model was used to study the biomechanical parameters of the lumbar spine in intact and instrumented cases. Various designs of instruments were applied to both the thoracic and the lumbar models. The effect of the instruments on the kinematic, i.e. range of motion (ROM), and kinetic, i.e. intradiscal pressure (IDP), facet load (FL), and ligament stress (LS), parameters of the lumbar spine and the thoracic spine were investigated. The lumbar instruments included posterior dynamic stabilization (PDS), fusion, interspinous fusion, and pedicle screws with spring rods. Design modifications were suggested after comparing the biomechanical behavior of the instrumented models with intact models.

Özet

Sonlu eleman metodu diğer alanlarda örneğin elektronik ve termodinamik bilimlerde olduğu gibi makine mühendisliği alanında da güvenilir bir analiz aracıdır. Biyomekanik alanında sonlu eleman modellerinin kullanımı bilgisayara dayalı kaynakların daha iyi kullanılabilirliği ile geçtiğimiz yirmi yıl içinde büyük bir ölçüde özellikle omurga biyomekaniği alanında artış göstermiştir. Aslında, omurga sonlu eleman modelinin gelişimi omurga bölümlerinin karmaşık geometri yapısından dolayı külfetli ve basit olmayan bir iştir. Sonlu eleman modelleri kas ve iskelet sistemlerinin davranışlarını yaklaşık olarak bütün fizyolojik ve anatomik özelliklerle birlikte hazırlamak için kullanılmaktadır.

Bu tezin başlıca amacı insana ait bel ve torakal omurga bölgelerinin gerçeğe yakın sonlu eleman modellerini geliştirmektir. Bel omurlarına (lomber bölgesine) ait sonlu eleman modelleri özellikle klinik tedavi uzmanlarının yanı sıra akademisyenler için de önemlidir. Çünkü bel ağrısı omurganın en sık görülen rahatsızlığını teşkil eder. Bu tezde omurga kemikleri ve diskleri arasında entegre ara yüz oluşturmak amacıyla özgün bir yöntem sunulmuştur. Bel ve torakal omurlarının gerçek geometrisi bilgisayarlı tomografi verilerinden elde edilmiştir. Boğum noktalarını omur kemiklerinin üzerine ve omur kemikleri arası disklerin yüzeyleri üzerine yerleştirmek amacıyla çok hücreli metot kullanılmıştır ve disk ve kemiklerin birleştirilmesi için altı yüzlü eleman kullanılmıştır. Bağ dokunun benzerini yapmak üzere iki boğum noktasını birleştirmek amacıyla çizgi şeklinde bir tür eleman olan “truss elemanı” kullanılmıştır. Omurların eklem yüzeylerinin birleştiği yerler tek yönlü ara elemanları ile tasarlanmıştır. Literatür verileri kullanılarak omurgayı oluşturan elamanlara göre madde özellikleri saptanmıştır. Net kuvvetler L1 vertebrasının üzerindeki tek noktaya uygulanmıştır. Her modeldeki son vertebranın alt kısmı bütün yönlerde bağlandı. Sonlu eleman modelinin ön görülen hareket tepkisi, bütün hareket eksenlerindeki yayımlanmış laboratuvar çalışmalarıyla ile karşılaştırıldı ve sonuçların benzer olduğu saptandı.

Geçerliliği kabul edilmiş sonlu eleman modeli bel omurlarının biyomedikal parametreleri üzerinde çalışmak amacıyla intakt ve aletli durumlarda kullanılmıştır. Aletlerin çeşitli tasarımları torakal ve bel omurga modellerine uygulanmıştır. Aletlerin bel ve torakal omurgalarının kinematik parametreleri üzerindeki etkileri; hareket aralığı ve kinetik gibi, disk içi basıncı, omurların eklem yüzeylerinin birleştiği yerlerdeki ağırlık ve bağ doku gerginliği gibi; incelenmiştir. Arka (posterior) dinamik stabilizasyonu, füzyon, omurların çıkıntıları arasında

bulunan (interspinöz) füzyon ve pedikül gibi özellikleri içeren bel omurga bölgesi aletleri yaylı bir çubuk ile sıkıştırılır. Tasarım değişiklikleri, aletli modellerin biyomekanik davranışlarının intakt modellerin davranışlarıyla karşılaştırılmasından sonra önerilmiştir.

To my parents

For their continued support throughout my academic years

Acknowledgement

I would like to acknowledge my advisor, Dr. Deniz Erbulut for his immense support and assistance over the course of two years. His sound knowledge and past research experiences about the spine biomechanics were valuable for me.

I would also like to thank Dr. Ali Fahir Ozer and Dr. Ismail Lazoglu for their assistance during my thesis work.

I would like to thank my project co-member, Iman Zafarparandeh for his continued support, especially in model generation and technical assistance with software.

I would like to thank TUBITAK for funding this project.

Also, I would like to thank Graduate School of Science & Engineering, Koç University for their administrative and logistical support.

I would like to thank my fellow graduate students in MARC lab for their support during my two years of Master's studies.

Table of Contents

List of Figures

List of Tables

Chapter 1 Introduction

Spinal pathologies are common, especially among elderly population of society. Spondylolisthesis, spinal stenosis, facet arthritis, disc bulging, and disc degeneration are some of the causes of low back pain. Over past several decades, advances in the medicine and engineering have led to better methods to deal with spinal pathologies. A range of devices for spine have been proposed in literature and tested using in vitro, in vivo, and finite element (FE) models. These devices can be categorized as artificial disc, interspinous process device, and fusion device. Biomechanical parameters, including range of motion (ROM), intervertebral disc pressure (IDP), facet stress (FS), ligament stress, and stress in posterior process are measured to quantify the effect of spinal devices on the spine kinematics. During past couple of decades, the usage of computational models as opposed to cadaver models has improved the validation of spinal devices as well as more precise measurement of biomechanical parameters.

The development of spine FE models has used a number of different methods. Each component of spinal column needs to be developed separately and verified before used for biomechanical analysis of surgical interventions and devices. The accurate geometry of the spinal bony components was extracted from computed tomography (CT) scans of healthy patients. Surface reconstruction of vertebrae and intervertebral disc was performed in Mimics software. These surfaces were exported to IA-FEMesh software for node assignment using multi-block method. A mesh was generated on the surfaces and later exported to ABAQUS for verification, ligament assignment, material property assignment, and implant of spinal devices. All kinematic analyses were performed in ABAQUS.

FE models of lumbar spine, L1-S1, and thoracic spine, T8-T9, were developed and used for several surgical case studies. The effect of graded facetectomy on the effect of lumbar spine ROM was studied. The load-sharing of lumbar spinal segments, including vertebra, intervertebral disc, facet joints, and posterior ligaments was predicted. An interspinous cylindrical process device was inserted at L3-L4 level and its effect on the ROM, FS, IDP and stress in posterior process were determined at instrumented and adjacent levels. Similarly, spring rod devices of two different designs were inserted at L4-L5 level and their effect was studied under hybrid loading. ROM, IDP, and FS were predicted at instrumented and adjacent levels. Two screw insertion angles were studied for thoracic spine: anatomic trajectory and straight-forward trajectory.

Cervical spine whiplash injuries are common in rear-impact road accidents. The effect of rear-impact on the biomechanical parameters of the lower cervical spine was studied under different headrest materials, backset, and acceleration magnitudes, using FE model. Image processing on the high frequency videos of the ATD tests was carried out to determine the angular change in the head-torso angle under 2 types of headrests and 4 acceleration magnitudes.

The aim of this thesis work was to develop and use accurate FE models for determining biomechanical properties of spinal components and devices. Chapter 2 provides a thorough literature review on determination of spine kinematics using different test methods, spine physiology, and posterior dynamic stabilization devices. Chapter 3 deals with finite element model generation, validation and determination of biomechanical properties of the model. Chapter 4 gives details of the two studies undertaken on posterior dynamic stabilization devices. Chapter 5 deals with the biomechanical effect of graded facetectomy. Chapter 6 provides whiplash injury study performed using image analysis of the dummy tests. Chapter 7 deals with thoracic spine modelling and instrumentation. Finally, Chapter 8 draws general conclusion of this thesis work.

Chapter 2 Literature Review

2.1. Introduction

Clinical and lab spinal kinematic studies have been in mainstream research for decades. Over the years, with the advancement in the computational methods and sensor technology, the kinematics of spinal components can be determined more precisely. Moreover, the devices for treatment of spinal pathologies can be evaluated for their effect on spinal components, distribution of load, and any damage to the spine after instrumentation, using the kinematics test methods. A detailed literature review of spine kinematics test methods, spine physiology, finite element models of spine, and Dynamic stabilization devices is given in this chapter.

2.2 Spine Kinematics Test Methods

2.2.1. In vitro

In vitro, or cadaver, test method involves components of spine procured from dead human beings. It is one of the most widely accepted methods of biomechanical testing for a device. Fresh cadaver spinal segments are modified by removing the accompanying muscles and connecting tissues. In some cases, radiographic evaluation is performed to rule out any specimen with fractures, degeneration, osteoporosis, or any other factor which effects mechanical properties of spine [1]. The cadaver samples are stored in cold environment (-20C), and carefully thawed before testing. The osteoligamentous structure of the spine is preserved to be used as an intact case. Depending on the case, if instrumentation is required, the device is inserted in the respective area of the cadaver by modifying the spine similar to actual surgical case. Figure 1 shows an in vitro testing setup with sensors.

However, cadaver testing is often not practical due limited resources, low precision of sensors, such as pressure plates, and moral and ethical issues involved. Moreover, cadavers cannot be used repeatedly and number of biomechanical parameters which can be measured is very limited. Therefore, other test methods are often explored.

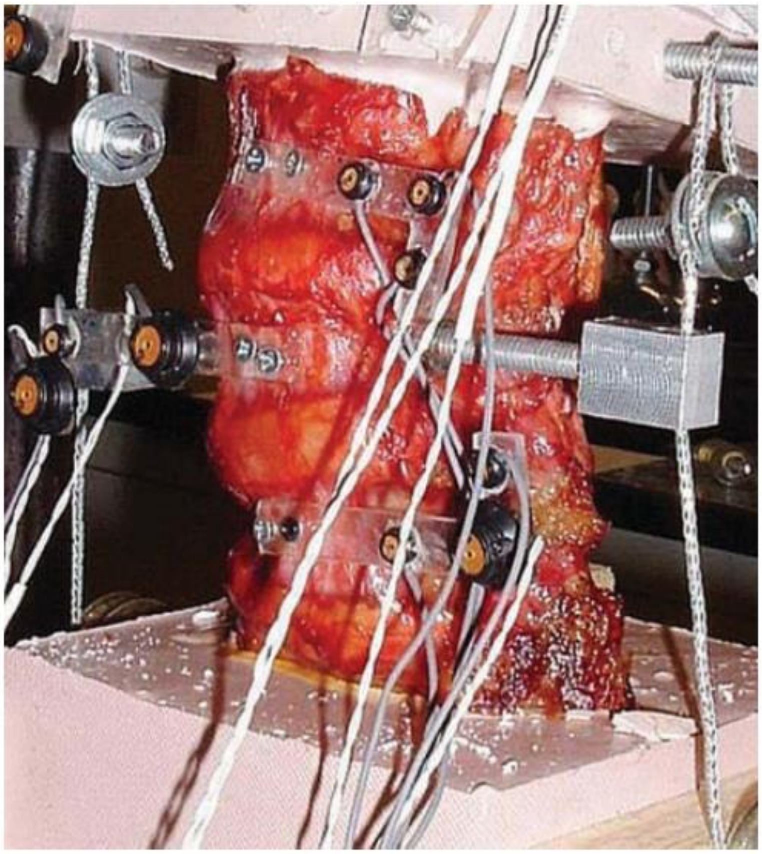

Figure 1: In vitro testing system [2]

2.2.2. In vivo

In vivo testing can either be evaluation of instrumented devices post-operatively, or performing kinematic tests on human volunteers. In case of volunteer studies, sensors are placed on the body externally. In some studies, the probes are inserted in the body by administering local anesthesia. Another method of in vivo testing is through radiography. X-Rays or CT scans are performed to post-operatively determine the condition and biomechanical parameters of the implants placed inside the body. Figure 2 shows the radiographic images for the lumbar posterior dynamic stabilization implant.

In vivo volunteer tests cannot be performed for extreme cases because of safety concerns. Moreover, the post-operative radiographs also provide very limited information; analysis of stress-strain is not possible in such cases.

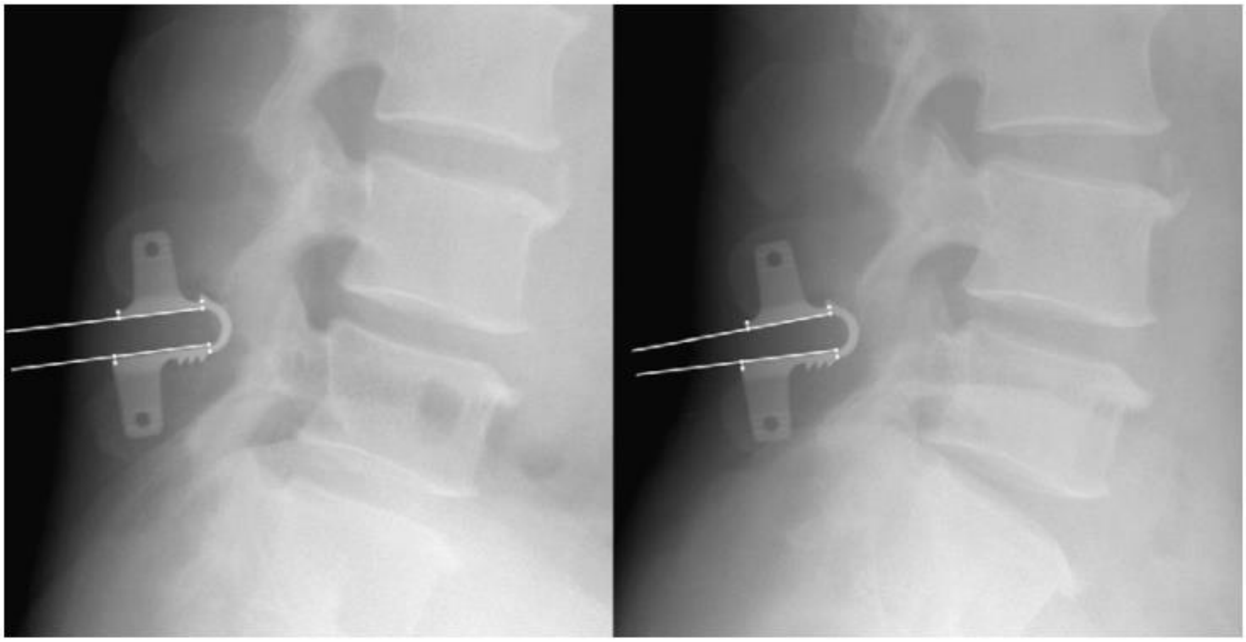

Figure 2: In vivo radiographs of the implant [3]

2.2.3. Anthropomorphic Test Dummy (ATD)

ATD tests are mainly used in crash tests such as in whiplash injury studies. A number of dummy models have been proposed for evaluation purposes, including rigid and flexible models [4]. ATD is helpful over other test methods because it takes into account the whole spine of the occupant [5]. Some of the commercially available ATDs are: BioRID and Hybrid-III (Humanetics Innovative Solutions, Plymouth, MI, USA). ATDs have been used in whiplash studies of car seat headrests [6] to test commercially available and newly designed headrests. Most commercially available ATDs, including those mentioned above, come along with sensors such as accelerometers and load cells. Figure 3 shows an ATD test being conducted for whiplash injury study. Such ATD tests allow experimentation of extreme conditions with availability of large amount of test data.

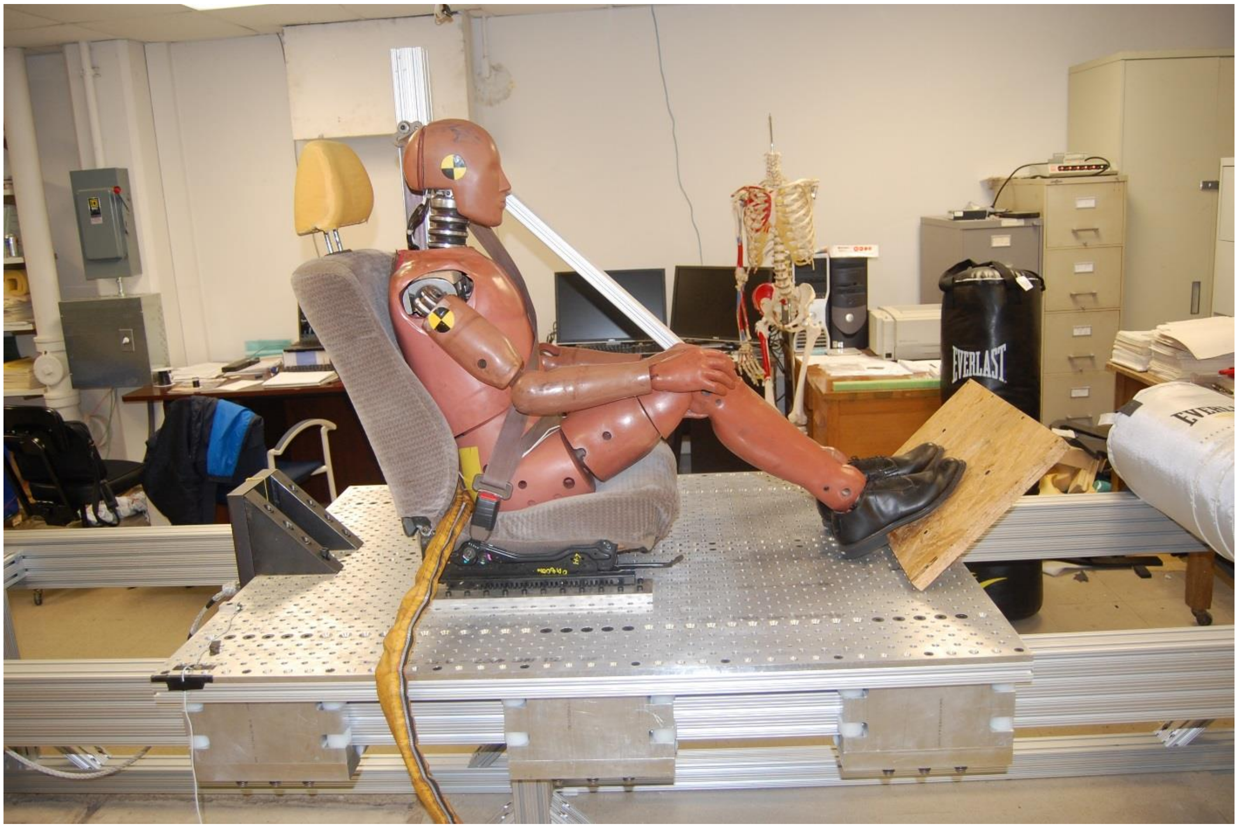

Figure 3: Anthropomorphic Test Dummy

2.2.4. Finite Element (FE) Model

FE models gained popularity by the end of last century, mainly because of development in computational methods and availability of better processors. However, the development of these models remains a difficult task because of spine unique biomechanical properties [7]. There are not many validated FE models existing at present time, especially for lumbar region which is clinically significant. These models are an alternative for in vitro and in vivo testing method because of low cost, greater flexibility in usage, ability to predict larger number of biomechanical parameters, less ethical concerns, incorporation of material nonlinearities, irregular loading, and availability of both geometrical and material domains [8,9]. Moreover, the isolated effect of biomechanical parameters can be studied using FE models.

However, FE models need to be validated before their usage in the clinical analysis of degenerative diseases and instrumentation devices [7]. The validation process includes comparison of FE model ROM values with cadaver ROM values in all planes. Only the stress analysis of a validated model under all normal loading conditions can be accepted clinically. The pure moments used for validation vary in each study but generally cervical models are validated in range of 0.5-2Nm [10] while lumbar models in the range of 7.5-15Nm [7].

The development of FE models involved various methods to determine accurate geometries of the structural components of the lumbar spine. Several studies used computed tomography (CT) scans of living [7,11,12] and cadaver human specimens [13,14,15,16,17] to obtain lumbar structural geometry. Other methods to obtain geometry include magnetic resonance imaging (MRI) which determines the structures that cannot be deciphered from CT scans [18]. In a study by Lee et al [19], digitizers were placed on the bony vertebral structures to acquire 3D coordinate data of lumbar structure. Of these methods, CT scans of living humans have been the most popular method of geometry extraction because of their subject-specific imaging and ability to provide accurate geometrical data [10].

FE models present in the literature can be classified either as symmetrical [13,16,20] or asymmetrical [10,14,21] across mid-sagittal plane. While asymmetrical models take larger development time, they capture the accurate geometry of the spine. This gives more credibility to the analysis performed using asymmetrical models.

2.3. Spine Physiology

Human spine can be broadly categorized in three sections: cervical, thoracic, and lumbar regions. The cervical region has 7 vertebrae, thoracic has 12 and lumbar has 5 vertebrae. The smallest functional unit of the spine is spinal motion segment [22]. Each such motion segment has the property of being viscoelastic, having both viscous and elastic properties which enables the spine to deform and recover when loaded and unloaded [22]. Almost all motion segments have same number of structures, described as follow:

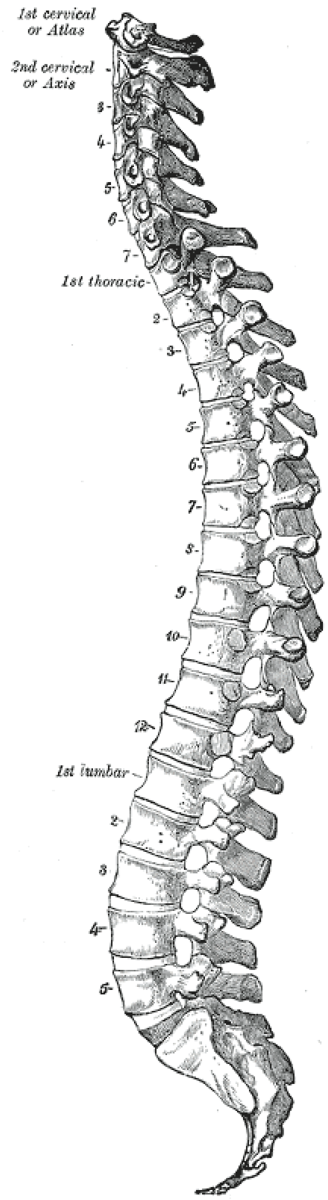

Figure 4: Spinal Column [23]

2.3.1. Vertebral body

The vertebral body is the main component of spine, a significant part in load-bearing of dpine [24]. Each vertebra is made up of cancellous bone core and cortical bone shell [25]. Cortical bone is resistant and less adaptive to deformation while cancellous bone can handle loads and deform without failure [22]. The size of vertebra increases down the spinal column, with cervical vertebra being smallest and lumbar vertebra being largest. Figure 5 shows a lumbar vertebrae with names of processes.

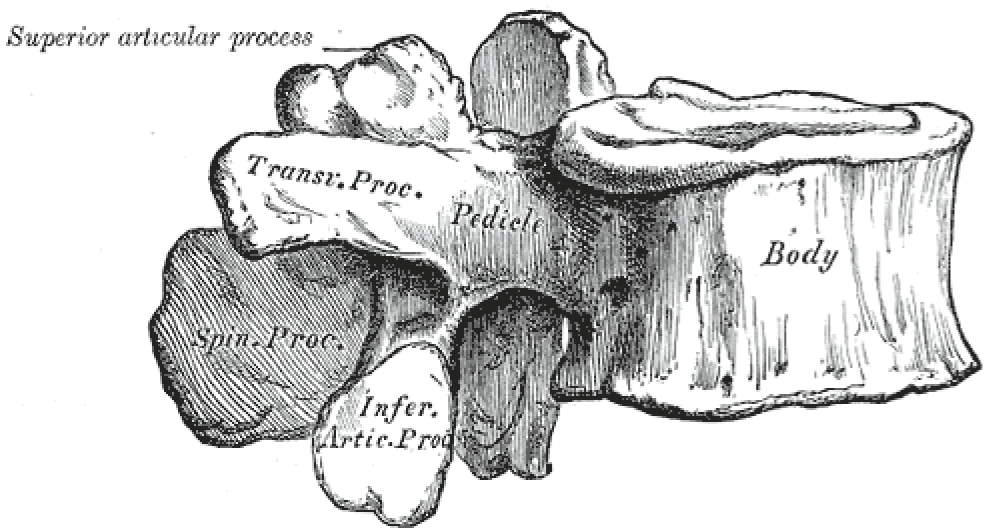

Figure 5: Lumbar vertebral body (side view) [23]

2.3.2. Intervertebral Disc

The intervertebral disc is the main component of spine which bears load. The disc consists of two distinct parts: the central nucleus pulposus and the surrounding annulus fibrosus, as depicted in Figure 6. The nucleus consists of large amount of hydrophilic proteoglycans [26]. Nucleus constitute 30-50% of the total disc volume, with the size in cervical and lumbar region greater than thoracic spine [25].

The annulus consists of high amount of collagen [26]. A complex system of fiber bundles, known as lamellae, make up annulus [22]. The arrangement of fibers is helicoid [25]. The fibers alternate direction in adjacent bands and are oriented at 30˚ to the disc plane [25]. These fibers become more compact on the outer side and differentiate into Sharpey fibers, combining with longitudinal ligaments [27].

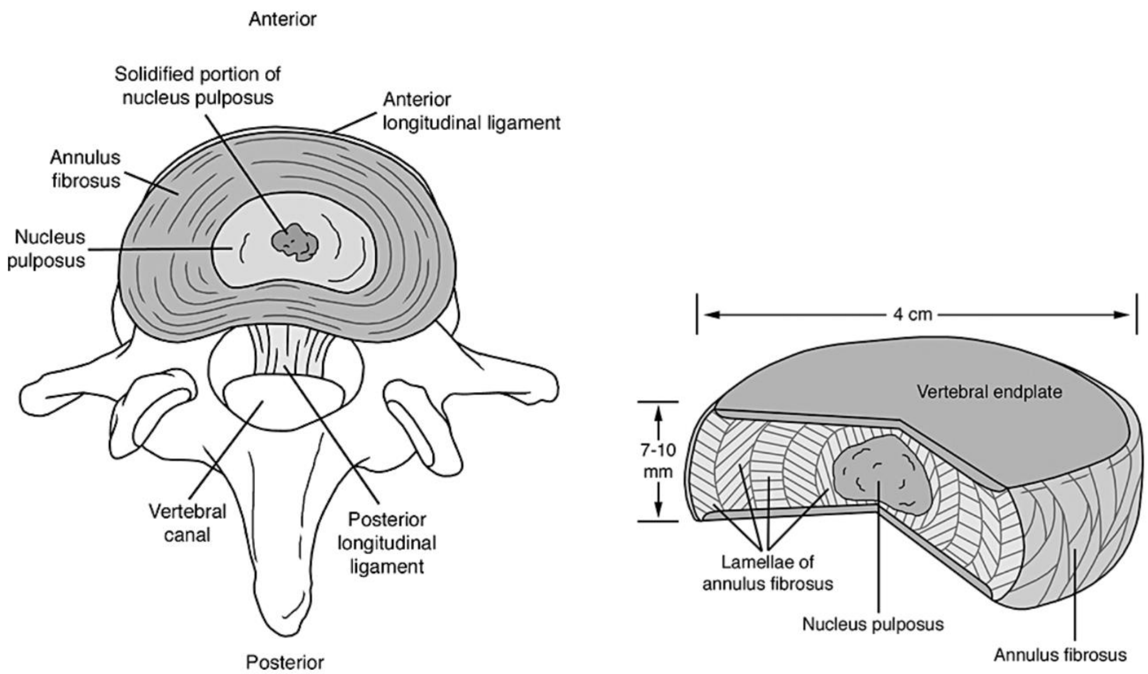

Figure 6: Lumbar Intervertebral disc anatomy [28]

2.3.3. Ligaments

Ligaments of spinal column are uniaxial structures and act non-linearly in response to loading [27]. There are six ligaments which are common throughout the spine while some ligaments are present only in upper cervical spine or lumbar regions (Figure 7). The functional significance of the ligaments is to allow sufficient physiologic motion with minimum usage of muscle energy [25]. Also, ligaments keep the motion within limits and, thus, prevent any trauma to the soft tissue by absorbing energy. The types of ligaments found in spinal column are described below.

The anterior longitudinal ligament (ALL) is attached between endplates of two adjacent vertebras and attached to the anterior side of intervertebral disk and vertebral bodies [22,25]. ALL can deform when disc bulges out [25]. Like disc, ALL degenerates with age [29], and can be disrupted in axial rotation [30].

The posterior longitudinal ligament (PLL) is attached on the posterior side of the intervertebral disc. It is less developed than ALL and merged into the collagen fibers of the posterior annulus of the disc [22].

The ligamentum flavum (LF) has thick and broad structures, connecting the laminae of the adjacent vertebrae [22]. LF are in pre-tension, that is, they are loaded in neutral position [31] which causes compression in the disc. By composition, LF has the highest percentage of elastic fibers in the body [31] due to which LF can undergo large amount of extension without permanent deformation. In case of sudden movement from full flexion to full extension, LF protects the spinal cord from any impingement [25].

Interspinous ligament (ISL) is thin membrane-like structure connecting adjacent spinous processes [25]. Supraspinous ligament (SSL) connects and passes along the tips of the vertebral spinous process [23].

Intertransverse ligament (ITL) connects adjacent thoracic and lumbar vertebral bodies on their lateral wings. They have very little mechanical function because their cross-sectional size is negligible [25]. ITL in thoracic region have higher failure stress but smaller failure strain as compared to other ligaments [32].

Capsular ligament (CL) surrounds the facet region, connecting adjacent vertebral posterior sections. CL are responsible for providing flexion stability in the cervical spine [33]. In thoracolumbar region, CL experience tension under axial loading as well [34].

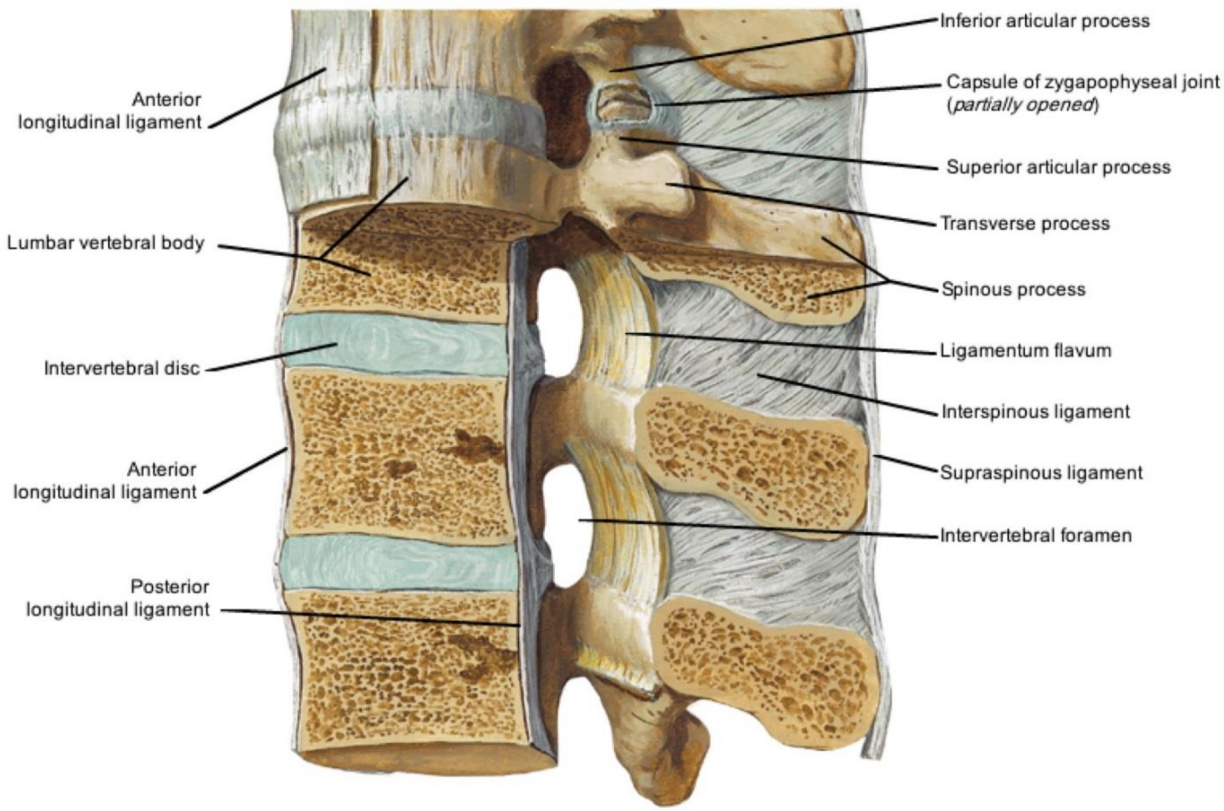

Figure 7: Ligaments of lumbar spine: side view [35]

2.3.4. Facet joints

The closest point of contact between two vertebral bodies is in posterior region where facet synovial joints are present. Facet joints are surrounded by capsular ligaments. The orientation of facet joints depend on the vertebral segment, changing from sagittal to coronal going down the spine. Facet joints allow large range of motion (ROM) in the flexion-extension plane while limiting motion in the lateral bending and axial rotation [36]. The facet joints are responsible for protecting lower lumbar disks from shear loads [37,38].

2.4 Finite Element Models of Spine

2.4.1. Lumbar Spine

Lumbar spine consisting of 5 segments is the lower part of spinal column. The vertebrae of lumbar are the largest in the spine. Ligaments present in lumbar include ALL, PLL, LF, ISL, ITL, SSL, and CL. Clinically, lumbar segments are of great significance because they bear most load of the upper body. Majority of spinal pathologies include low back pain which arises from disk degeneration, spondylolisthesis, and disk bulging.

Several FE models of lumbar spine have been proposed in literature [8,13,14,16,20]. These models vary in material properties and loading conditions. The ROM of lumbar FE motion segment is found to be affected by disc height [39,40] and material properties [41]. The loading conditions must be related with *in vivo* motion for routine tasks [42]. FE models of lumbar spine present in literature vary in their material properties, symmetry along mid-sagittal plane, simulation of facet joints, loading conditions, and number of segments. Some of the model have been presented below.

The cortical bone in the most FE models has elastic material property with value of E in range of 10000-12000 MPa, approximately [13,14,43]. Similarly, the cancellous bone was modelled by elastic material properties in most FE models with value of E in range of 100-200MPa. For posterior bony elements, a value of E=3500MPa has been used in most of the reported FE models. However, Shirazi-Adl [17] used a rigid cortical, cancellous and posterior bone.

The nucleus pulposus of intervertebral disc is considered as incompressible fluid filed cavity in previously developed FE models [11,12,15]. Ayturk and Puttlitz [14] modelled nucleus using an elastic material with E=1.0MPa. Modelling of annulus fibrosis is a difficult task and there is several different material properties used in literature. The ground substance of annulus was given hyperelastic material property such as Neo-Hookean [13] and Mooney Rivin [15,16,43]. Fibers of annulus have been modelled in various ways. Kiapour et al. [13] used 8 layers of fiber-reinforced continuum elements with crisscross pattern. Schmidt et al. [16] had 16 layers of crisscross pattern with non-linear stress-strain curve. Other models used non-linear distance dependent layers with crisscross patterns [11,43].

Modelling of ligaments has been done is various ways. Majority of models reported in literature simulated ligaments through non-linear stress-strain curve [11,15,16,43]. Kiapour et al. [13] used uniaxial 2D elements wuth defined cross-sectional area and non-linear hypoelastic properties.

Ayturk and Puttlitz [14] simulated ligaments through exponential force-displacement curves while Liu et al. [12] used linear stress-strain curve.

Similarly, modelling of facet joints was performed in various ways in the reported models. Some models simulated facets as hard frictionless contact with Young Modulus in the range of 10-35 MPa and initial gap of around 0.5mm [11,16]. Ayturk and Puttlitz [14] used neo-Hookean for facet joints. Other models used soft frictionless contact with varying value of gap [12,13,17,43]. Some of the FE models present in the literature are shown in Figure 8.

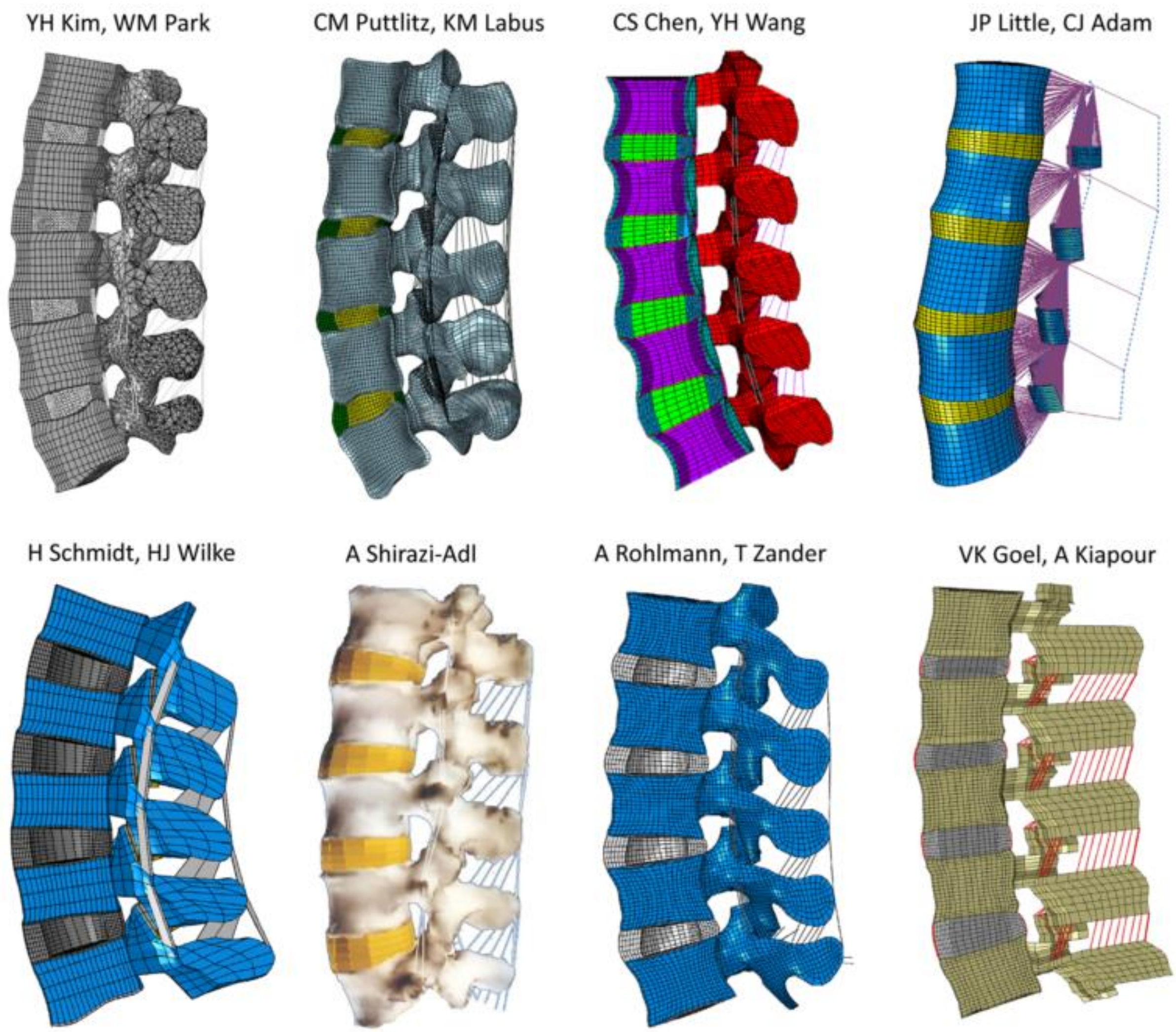

Figure 8: Finite element models present in literature [44]

2.5. Dynamic Stabilization Devices

The lumbar degenerative diseases have been treated conventionally through spinal fusion. However, fusion in the treatment of lower back pain has been reported for adjacent segment disease in long-term clinical follow-up [45,46,47]. This has led to increase in demand and development of dynamic stabilization devices, especially in patients suffering from multi-segment disc degeneration [48].

Posterior Dynamic Stabilization (PDS) devices change the movement and load transmission of a spinal motion segment without fusion of segments [48]. It serves the purpose of limiting motion in one plane while keeping motion unchanged in other planes of motion [49]. PDS leaves the spinal motion segment mobile, unlike fusion, and only alters the load bearing pattern of the spine segment. The main benefit of such devices is that they prevent adjacent level degeneration [48,50]. Dynamic stabilization devices can be broadly divided into following categories: interspinous process devices; interspinous ligament devices; pedicle fixation-based screw systems; and semi-rigid metallic devices across the pedicle screws [48].

Interspinous process (ISP) devices are implanted as a surgical treatment for different types of spinal pathologies, such as spinal stenosis or facet arthritis [51,52]. These devices are floating in nature, that is, they are not rigidly connected to the vertebrae. The main design goal of such devices is to apply a distraction force to the processes and prevent further extension of the segment [53]. Some of the popular ISP devices are: Coflex (Paradigm Spine), Wallis (Abbot Spine), DIAM (Medtronic), and X-Stop (Saint Francis Medical Technologies Inc.). Of all ISP devices, the X-Stop device (Figure 9) has been documented most extensively in the literature [54]. It has 2 lateral wings to prevent unnecessary displacements [55]. Its design is aimed mostly at preventing extension while allowing normal motion in other motion planes.

Figure 9: X-Stop interspinous process device [55]

Pedicle fixation-based PDS systems have two components: screws, which are inserted in the pedicles of vertebrae from posterior side; and rods, which are inserted between two screws. Various designs of both screws and rods have been suggested in literature. The Dynesys system (Zimmer Spine) is a pedicle screw-based PDS system for dynamic or semi-rigid stabilization of lumbar spine. Figure 10 shows the Dynesys system. The design objective of this system was to limit abnormal forces, restore lumbar spinal functions and limit adjacent segment degeneration [47]. The system consists of titanium alloy pedicle screws which are connected by polyethylene terephthalate longitudinal cord.

Figure 10: Dynesys PDS system [47]

Another pedicle screw based PDS system is a spring rod of Nitinol shape memory alloy (BioFlex System; Bio-Spine) and was developed in Korea [56]. The rod has diameter of 4 mm, with coiled shapes taking one or two turns, as shown in Figure 11. The system brings stability during flexion, extension, and lateral bending in lumbar [56].

Figure 11: BioFlex Nitinol PDS system [57]

Chapter 3 Finite Element Model Generation

FE models of complete lumbosacral (L1-S1) and thoracic (T8-T9) spine were developed as part of thesis work. Moreover, upper cervical spine ligament attachment was carried out in this study. Mesh development was achieved though multi-block technique and geometry was obtained from computed tomography (CT) scans. The development procedure was divided in three parts: 1) Surface Extraction; 2) Mesh Generation; and 3) Material Properties Assignment. Detailed procedure of FE model generation has been given below:

3.1. Surface Extraction

The geometry of the lumbar vertebrae was obtained from CT scan data for a healthy 35-year-old man [53,58]. An example of CT scan used for surface extraction is shown in Figure 12. The image processing of CT scans was done in software Mimics® (Version 14.1; Materialise, Inc., Leuven, Belgium). Bony structures of lumbar were segmented using masks which gave three-dimensional surfaces of vertebra. The accurate geometry of the lumbar was preserved by using the exact shape of lumbar components as they were present in scans. Since intervertebral discs were invisible on CT scans, they were manually created by inserting three-dimensional surface between two adjacent vertebral endplates [10]. Figure 13 shows vertebra and intervertebral extracted surfaces for lumbar L1-L5.

Figure 12: CT scan of lumbosacral spine in sagittal plane.

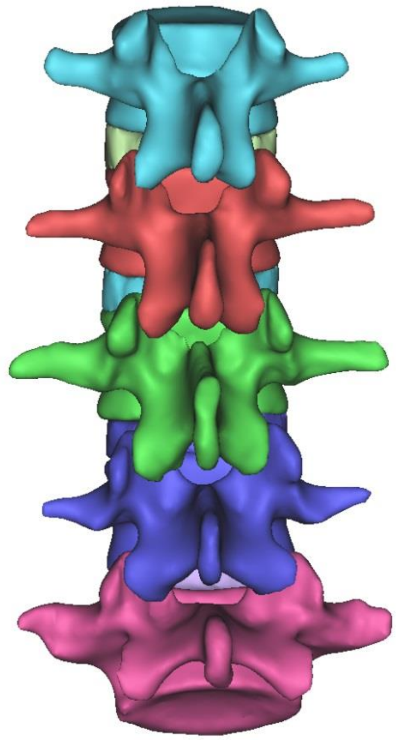

Figure 13: Surface reconstruction of lumbar spine

3.2. Mesh Generation

The surfaces reconstructed in the previous step were exported in STL format. A multi-block technique was adopted to create mesh in less time, as proposed by Kallemeyn et al. [59]. The blocks were created in the software IA-FEMESH (University of Iowa, IA, USA). Volumetric hexahedral mesh of the vertebra and intervertebral discs was created using blocks. The final mesh of each part was lumbar segment was imported into ABAQUS® (Version 6.10-2; Abaqus, Inc., Providence, RI, USA). Adjoining vertebras and intervertebral disc were merged at the boundaries to create a continuous lumbosacral structure.

Figure 14 shows FE mesh of L3 vertebra. The central body and the posterior processes were assigned block separately and these block were merged later. Intervertebral disc mesh is shown in Figure 15. Nodes were placed radially and a radial mesh was generated which helps in assigning annulus fibers.

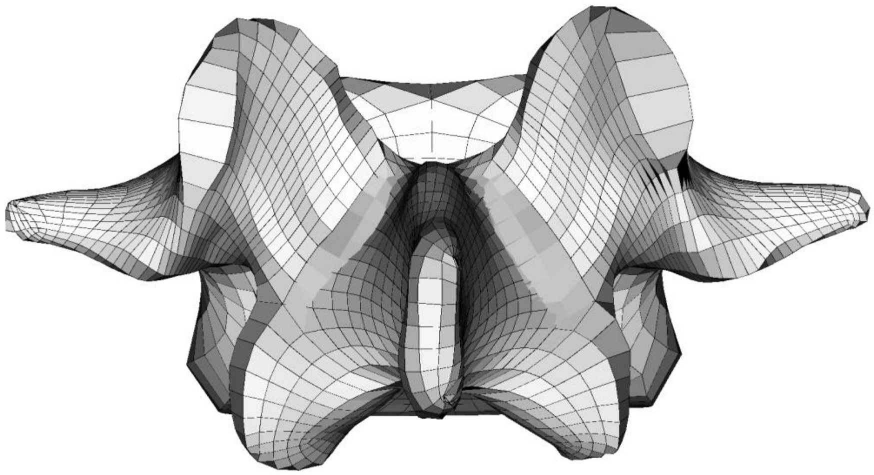

Figure 14: FE mesh of L3 vertebra

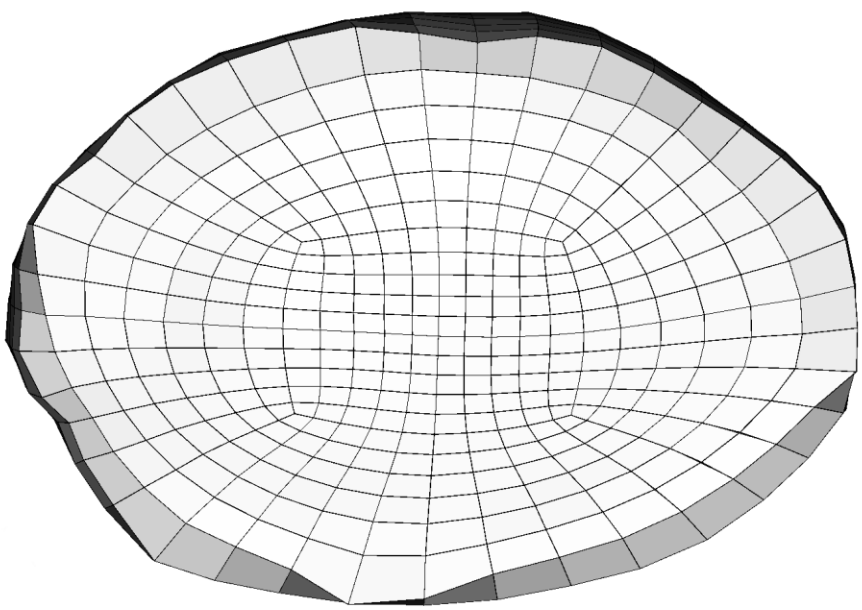

Figure 15: FE mesh of intervertebral disc

FE model of an intervertebral disc consisted of two components: the nucleus pulposus and the annulus fibrosus. The disc was meshed in a circular mesh pattern which helped in modelling of concentric rings of annulus ground substance. The rebar element option in ABAQUS was used to model the annulus fibers, oriented at $\pm 30^{\circ}$. The fibers were restricted under tension loading only. The annulus was modelled by hyperelastic material. The nucleus was modelled as a fluid by using a hexahedral element with a very low stiffness (1 MPa) and near-incompressibility (Poisson's ratio υ =0.4999).

Ligaments were modeled using two-dimensional truss elements. Each ligament was assigned a specific cross-sectional area and the number of elements for each ligament was varied such that total cross-sectional for a ligament complies with anatomy values. All seven ligaments including ALL, PLL, LF, ITL, ISL, SSL, and CL were created using truss elements for lumbar and thoracic segments. The ligaments were simulated using hypoelastic material to model their stiffness with respect to strain.

Gap contact elements (GAPUNI) were used for facet apophyseal joints. GAPUNI elements propagate force in a single direction as a function of gap between nodes [10]. Each side of lumbar motion segment was modelled by 8 GAPUNI elements. The stiffness and cross-sectional area of each element was varied to obtain anatomical value.

3.3. Material Properties Assignment

The complete FE models of L1-S1 and T7-T9 were asymmetric across mid-sagittal plane. L1-S1 consisted of 72193 nodes and 55650 elements. Figure 16 shows complete FE model of lumbosacral spine. Figure 17 shows FE model of T7-T9. Material properties were assigned to each spinal component using values from literature [60]. Table 1 summarizes these material properties.

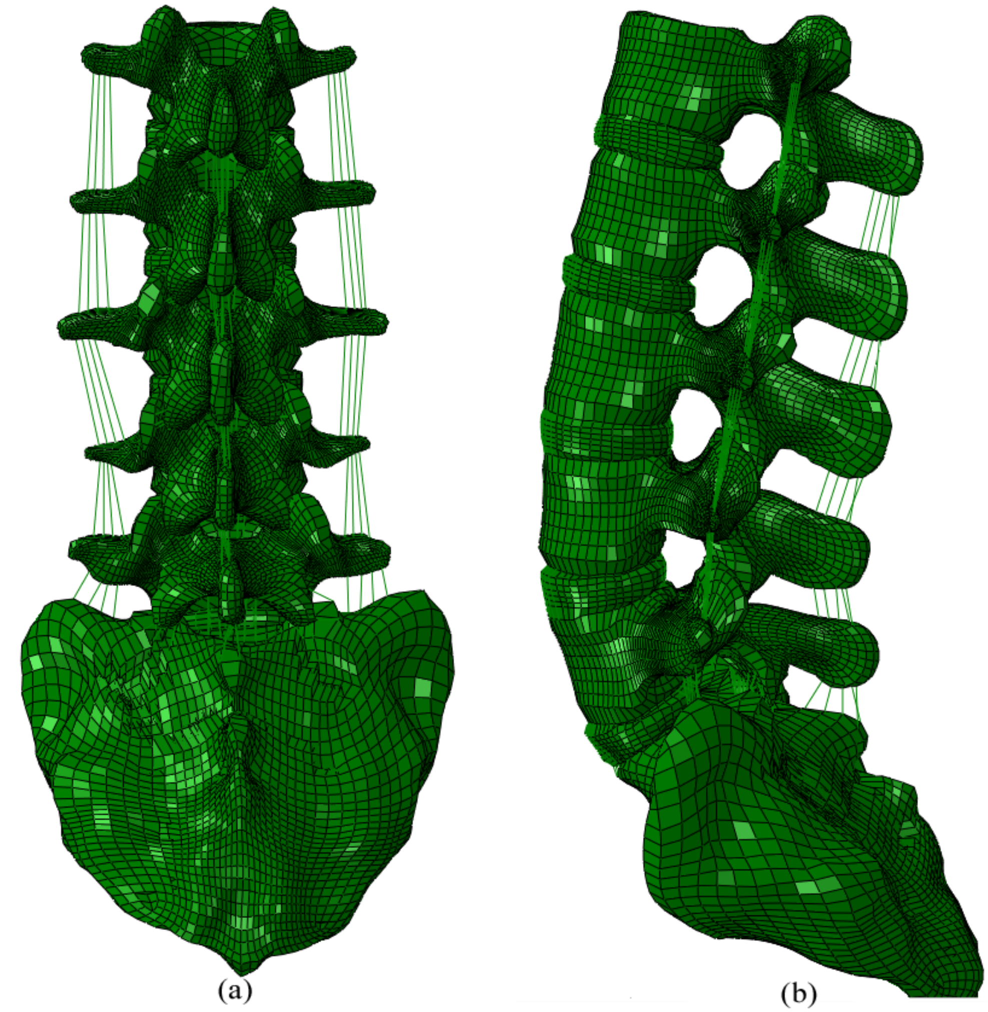

Figure 16: Lumbosacral FE model (a) frontal and (b) sagittal views

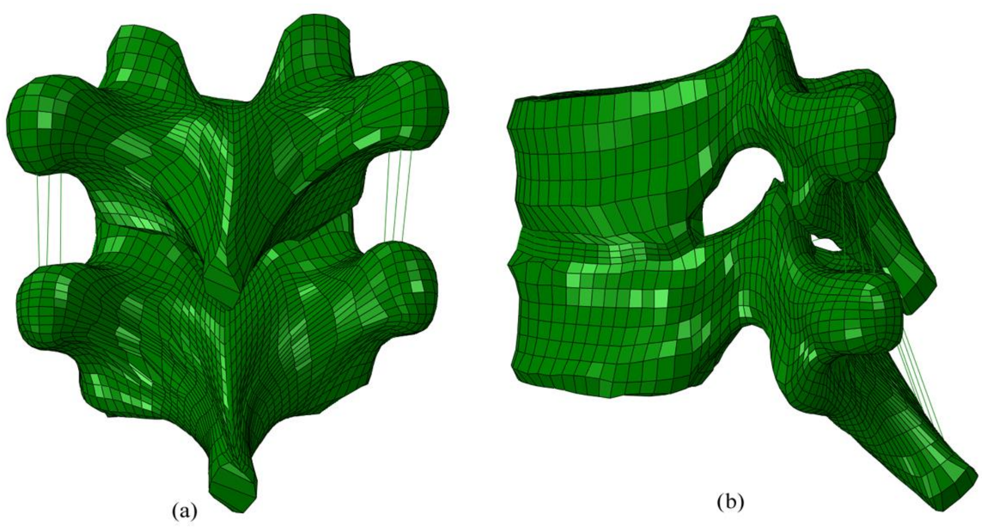

Figure 17: T8-T9 FE model (a) frontal and (b) sagittal views

Table 1: Material Properties of the lumbar spine components, as derived from literature [13].

Component	Element Formulation	Modulus (MPa)	Poisson's Ratio
Vertebral Cancellous Bone	Isotropic, elastic hex elements	450	0.25
Vertebral Cortical Bone	Isotropic, elastic hex elements	12000	0.3
Posterior Bone	Isotropic, elastic hex elements	3500	0.25
Nucleus Pulposus	Isotropic, elastic hex elements	9	0.4999
Annulus (Ground)	Hyperelastic, Neo Hooke	C10=0.3448, D10=0.3	
Annulus (Fiber)	Rebar	357-550	0.3
Ligaments			
Anterior Longitudinal	Truss elements	7.8 (<12%), 20.0 (>12%)	0.3
Posterior Longitudinal	Truss elements	10.0 (<11%), 20.0 (>11%)	0.3
Ligamentum Flavum	Truss elements	15.0 (<6.2%), 19.5 (>6.2%)	0.3
Intertransverse	Truss elements	10.0 (<18%), 58.7 (>18%)	0.3
Interspinous	Truss elements	10.0 (<14%), 11.6 (>14%)	0.3
Supraspinous	Truss elements	8.0 (<20%), 15.0 (>20%)	
Capsular	Truss elements	7.5 (<25%), 32.9(25%)	0.3
Apophyseal Joints	GAPUNI		

3.4. Results

3.4.1. Validation

The lumbar FE model was validated with respect to cadaver studies [61,62,63,64] in three motion planes. Table 2 shows comparison of in vitro and FE model predicted values of range of motion (ROM) for three planes of motion. Both left and right axial rotation and lateral bending were validated separately because the model was asymmetric across mid-sagittal plane. ROM of FE model for flexion was stiffer than *in vitro* studies, particularly at L1-L2, L3-L4, and L5-S1. Extension ROM was generally within the standard deviation of the cadaver values, except L5-S1 where FE ROM was found to be stiffer.

3.4.2. Facet Load (FL)

FL was highest in extension and axial rotation where FL reached 200N on at least one side of facet joints. Flexion had least effect on FL as loads were less than 25N on either side of facet joints. In left lateral bending, 21N and 79N were predicted for left and right facets, respectively. In right lateral bending, 67N and 21N were predicted for left and right facets, respectively.

3.4.3. Intradiscal Pressure (IDP)

Maximum IDP was predicted for L4-L5 disc nucleus in each motion plane. The least IDP of 0.90MPa was predicted for extension motion. For flexion motion, it increased significantly to 1.67MPa. Similarly, left and right axial rotations had IDP of 1.42MPa. The highest IDP was predicted for lateral bending where 2.14MPa and 2.31MPa for left and right lateral bending, respectively, were recorded.

3.4.4. Ligaments

Two ligaments were investigated for load sharing analysis. For interspinous ligament (ISL), the highest stress of 3.27MPa was predicted in flexion followed by 0.7MPa in axial rotation. There was insignificant effect of ISL in extension and lateral bending (<0.001MPa). Capsular ligaments (CL) had considerable effect in flexion where highest stress of 29MPa was predicted.

Table 2: Validation of the FE model against in vitro studies

	Flexion	**Extension**	**Lateral Bending**	**Axial Rotation**
L1-L2				
Yamamoto et. al [65], 10Nm	5.8±0.6	4.3±0.5	4.7±0.4 (L) 5.2±0.4 (R)	2.6±0.5 (L) 2.0±0.6 (R)
Present Study, 10Nm	3.2	4.1	6.7 (L) 7.2 (R)	3.9 (L) 3.4 (R)
L2-L3				
Schmoelz et al [66], 10Nm	4.3±1.0	4.6±2.2	5.4±2.2	1.0±1.0
Yamamoto et. al [65], 10Nm	6.5±0.3	4.3±0.3	7.0±0.6 (L) 7.0±0.6 (R)	2.2±0.4 (L) 3.0±0.4 (R)
Present Study, 10Nm	3.9	2.9	5.9 (L) 6.4 (R)	3.2 (L) 3.4 (R)
L3-L4				
Niosi et al [67], 7.5Nm	4.4 ±2.0	2.4 ± 0.9	2.4 ± 1.2	1.2 ±0.5
Schilling et al [68], 7.5Nm	4.67±1.79	2.18±0.54	7.66 ±2.91	4.67 ±2.52
Schmoelz et al [66], 10Nm	5.0±1.0	4.0±1.3	4.7±2.0	1.0±0.6
Yamamoto et. al [65], 10Nm	7.5 ±0.8	3.7 ±0.3	5.7 ±0.3 (L) 5.8 ± 0.5 (R)	2.7 ± 0.4 (L) 2.5 ±0.4 (R)
Present Study, 10Nm	3.5	3.6	6.2 (L) 7.4 (R)	3.6 (L) 3.8 (R)
L4-L5				
Schilling et al [68], 7.5Nm	5.62 ±2.17	3.32 ±1.12	7.76 ±1.85	5.16±1.30
Yamamoto et. al [65], 10Nm	8.9 ±0.7	5.8 ±0.4	5.5 ±0.5 (L) 5.9 ±0.5 (R)	1.7±0.3 (L) 2.7±0.5 (R)
Present Study, 10Nm	5.0	3.2	6.4 (L) 7.1 (R)	4.0 (L) 3.9 (R)
L5-S1				
Yamamoto et. al [65], 10Nm	10±1.0	7.8±0.7	5.3±0.4 (L) 5.7±0.4 (R)	1.5±0.2 (L) 1.3±0.2 (R)
Present Study, 10Nm	8.5	3.0	6.2 (L) 7.3 (R)	8.4 (L) 4.6 (R)

Extension had moderate effect on CL, with maximum stress of 20.7MPa. Left axial rotation had maximum predicted stress of 21MPa while right axial rotation had maximum predicted stress of 30MPa on CL. In left lateral bending, the predicted stress on CL was 16MPa which decreased significantly to 0.6MPa in right lateral bending.

3.5. Discussion

The aim of this study was to develop an asymmetric FE model of lumbar, all through L1 to L5. Validation of model was carried out against literature values of *in vitro* studies. In general, the predicted ROM values of FE model closely followed cadaver values. However, in case of flexion, FE model showed stiffness and, consequently, lower ROM than *in vitro* ROM values of Yamamoto et al. [69]. In axial rotation and lateral bending, deviations from *in vitro* values were observed. A couple of reasons are being suggested for such behavior. Firstly, *in vitro* studies mostly involve lumber from an elderly person who has degenerations in motion segments. Secondly, intervertebral discs, which play an important part in load transfer during lateral bending, axial rotation and flexion, have variable degeneration during *in vitro* testing [70]. Hence, a difference between cadaver and FE model ROM values was observed during validation.

After validation of the lumbar FE model, load sharing ability of some of its components was tested in all three planes of motion. In first phase, the role of facets was studied. Kiapour et al. [13] investigated effect of facetectomy on a FE lumbar spine and concluded that only extension and axial rotation are significantly affected by facet removal. Sharma et al. [71] reported results of facet removal on flexion and extension motion only. Their FE model predicted moderate facet stresses in flexion because of resistance provided by capsular ligaments. For extension, they reported high facet stresses due to contact between articular surfaces. Similarly, the results of current asymmetric model showed that facet joints were loaded to significant values in extension and axial rotation only.

In the second phase, role of intervertebral disc was investigated. To analyze the effect of intervertebral disc on the lumbar motion, Panjabi et al. [72] performed cadaver testing. Discectomy was carried out and its effect on mechanical behavior of lumbar was recorded. Their results showed that nucleus removal strongly affects the flexion and right lateral bending with moderate effect in axial rotation and minimal change in extension. The results predicted by our FE model have positive correlation with *in vitro* test data. Lateral bending exerts most pressure on intervertebral disc nucleus, followed by flexion. Therefore, it can be concluded that these two motion planes transfer most load to disc nucleus.

The third phase of this study involved analysis of two posterior ligaments on the motion of lumbar. Sharma et al. [71] discussed role of posterior ligaments in their symmetric FE model study. Their investigation concluded that flexion has significant dependence on ligaments, especially ISL and CL. In extension motion, there was limited effect of CL removal alone. However, when facets were removed along with CL, it produced a large increase in extension motion. Hence, it was proposed by Sharma et al. [71] that ISL in flexion and CL in extension transfer most of the load.

One of the distinctive features of proposed FE model was asymmetry of facet planes along mid-sagittal plane. This non-alignment of facets led to coupled motion, reported in our previous study [73]. The coupled motion was prominent in extension where some of the motion was observed outside sagittal plane. This feature is particularly significant for future studies involving surgical or pathological conditions.

Chapter 4 Posterior Dynamic Stabilization Device Analysis

Posterior dynamic stabilization (PDS) devices are used to limit the spinal motion in a specified plane and cause minimal adjacent level degeneration. As part of current study, two cases of PDS were considered: a cylindrical ISP device, and two pedicle screw based spring rods with different designs. In each case, intact and instrumented models were analyzed for kinematic and kinetic biomechanical parameters.

4.1. ISP Device

The ISP device, X-Stop, has been documented most in the literature owing to its simpler design. In an in vitro study, Lindsey et al. [74] investigated the effect of X-Stop implantation on the kinematics of implanted and adjacent segments and found that it significantly reduced the range of motion (ROM) in extension at the implanted level while retaining the ROM in flexion, axial rotation, and lateral bending. They also found that the device did not affect the ROM of the adjacent segments in any motion direction. In another in vivo study, Siddiqui et al. [75] investigated the changes in disc height and segmental and total lumbar rotation before and after X-Stop implantation and concluded that the disc height and sagittal kinematics of the lumbar spine are not significantly affected by the device.

Wilke et al. [76] compared the effects of 4 interspinous implants—Coflex (Paradigm Spine), Wallis (Abbot Spine), DIAM (Medtronic), and X-Stop—on ROM and intradiscal pressure (IDP) in an in vitro test in which pure moments were applied on a functional spinal unit in flexion-extension, lateral bending, and axial rotation. Their results showed that all implants reduced ROM in extension by about 50% of that in the intact model. However, none of them affected ROM in other directions. Further, as was the case with ROM, all implants reduced IDP in extension but did not have any effect on it in other directions. In another in vitro study, Hartmann et al. [77] studied the biomechanical effect of 4 interspinous implants—Aperius (Kyphon), In-Space (Synthes), X-Stop, and Coflex—on the ROM at implanted and adjacent levels using L1–L5 cadaveric specimens. They found that all 4 devices caused a significant reduction in ROM in extension but did not affect it under pure moments in other directions. They also showed that when a follower load was applied with pure moments, the ROM in flexion decreased for all 4 implants. Wiseman et al. [78] determined the effect of an implanted X-Stop device on the facet load in extension at the index and adjacent segments of L2–L5 cadaveric specimens and found a significant reduction in facet loads at the index level but no change in the loads at the adjacent level. Swanson et al. [79] investigated the influence of X-Stop implantation on the IDP at the index (L3–L4) and adjacent levels in vitro. They observed that the device did not significantly affect IDP at the adjacent level, although it was decreased considerably at the index level.

All the above-mentioned studies were in vitro; however, in vitro investigations have several limitations. For example, as reported by Wilke et al., [76] the IDP in vitro may not be calculated correctly by using pressure transducers. However, finite-element (FE) studies, unlike in vitro studies, can help researchers to examine the inner workings of the lumbar spine and study the effects of an ISP device on load sharing, stresses, and strains in the spine under different loading conditions. To this end, Lafage et al. [80] conducted a combined in vitro and FE study to investigate the effect of the Wallis implant on ROM and stress at the disc annulus and implant at the index and superior adjacent levels. They used the L3–L5 segments for cadaver and FE studies and observed a reduction in motion and disc internal loads in the case of the implanted segment. However, their model was limited to studying the adjacent-segment effect since it had just 2 segments. Furthermore, they applied a flexible protocol (load control) instead of a hybrid protocol (displacement control). The latter is more anatomically relevant and can better represent the motion and loads experienced by the spine after surgical procedures and implantation [20,81]. However, in the field of ISP devices, no study has utilized the FE approach for a detailed biomechanical investigation of the effect of these devices on adjacent segments by using a hybrid protocol.

Therefore, a FE study was carried out to evaluate the effect of an implanted ISP device on the biomechanical parameters of a lumbar spine by using a hybrid testing protocol. The biomechanical parameters considered were ROM, IDP, and facet load at both the index and the adjacent level. In addition, stress in the ISP device after implantation was evaluated.

4.1.1 Material & Methods

The FE model of the lumbar spine, developed as part of this thesis work, was used in this ISP study. An ISP device was inserted between the ISPs of the L3 and L4 segments; the design of this device, which was the static kind, was similar to X-Stop in that the cross-section of the device was oval (Figure 18). The device had a core that could be accommodated between the processes without any injury to the ISL and SSL. Two wings were designed to keep the device in place. The upper elements of the device were coupled to adjacent elements on the processes of the corresponding vertebra. Titanium alloy was selected as the material for the device. The isotropic elastic formulation was used to simulate the material properties of titanium (Young's modulus 115 GPa, Poisson's ratio 0.3).

The implanted model was loaded in all 3 main directions: flexion-extension, lateral bending, and axial rotation. A hybrid protocol, which was used in all simulations, was implemented with the aim of examining adjacent-segment biomechanics by varying the moment until the overall deflection of the implanted L1–L5 model equaled the predicted deflection for the intact model [81,82]. The hybrid moment for the implanted model was 14.5 Nm in extension. A bending moment of 10 Nm was used in all other directions because similar total ROMs were obtained in other motion directions

4.1.2. Results

Figures 19-22 show the ROM at each lumbar level for both the intact and implanted models in extension, flexion, lateral bending, and axial rotation, respectively. In the extension direction, ROM at the L3–L4 segment decreased by 80.6% after implantation relative to the ROM at this segment in the intact lumbar spine. Further, the ROM values in adjacent segments—that is, L2–L3 and L4–L5—increased by 29.7% and 21%, respectively, relative to those in the corresponding segments in the intact spine.

At the index level, ROM changed by up to 8% and 3% in lateral bending and axial rotation, respectively, but it did not change in flexion. At the adjacent level, the change in the ROM was the same—by up to 2%—in flexion, lateral bending, and axial rotation.

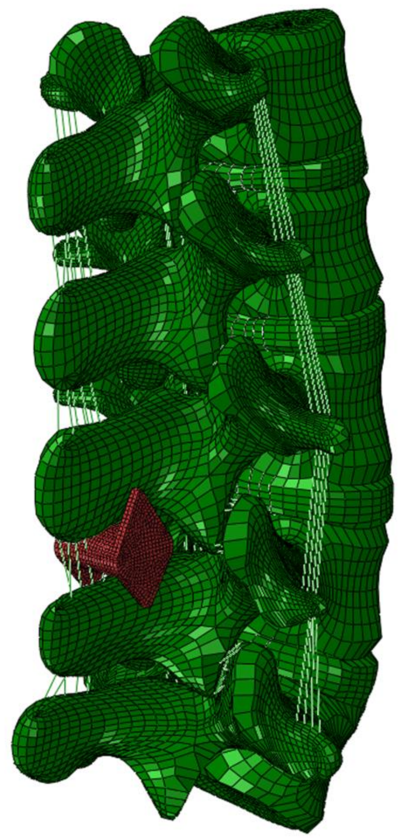

Figure 18: L1-L5 FE model with ISP device at L3-L4 level.

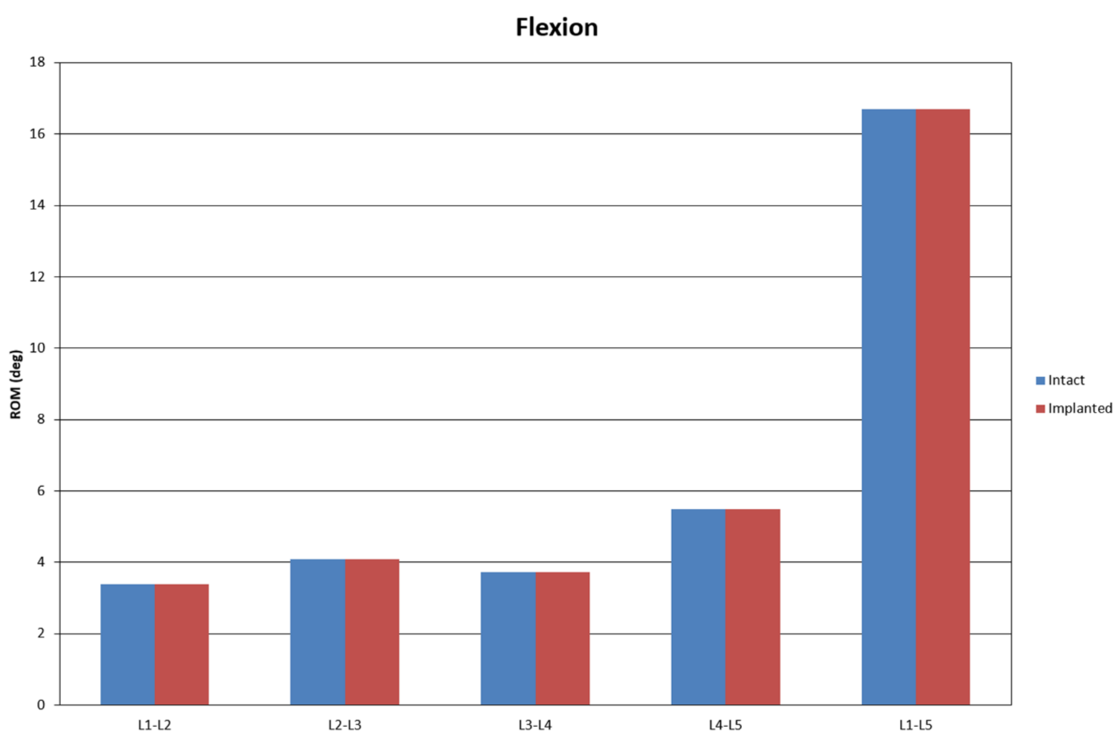

Figure 19: Hybrid flexion ROM for intact and implanted model

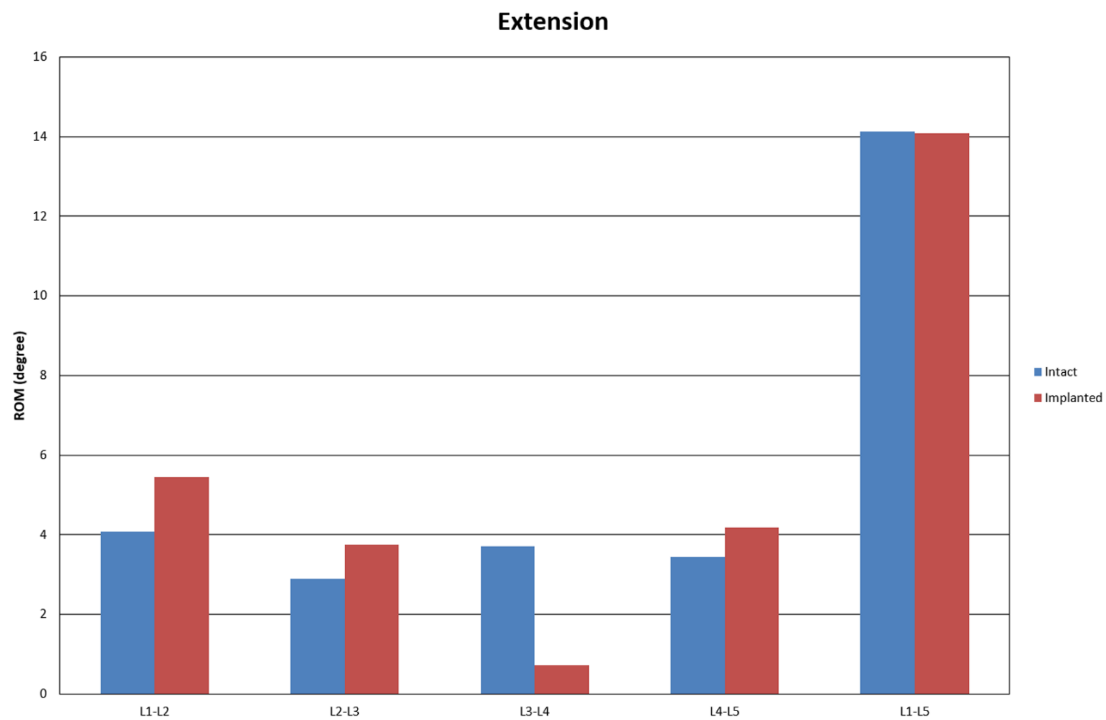

Figure 20: Hybrid extension ROM for intact and implanted model

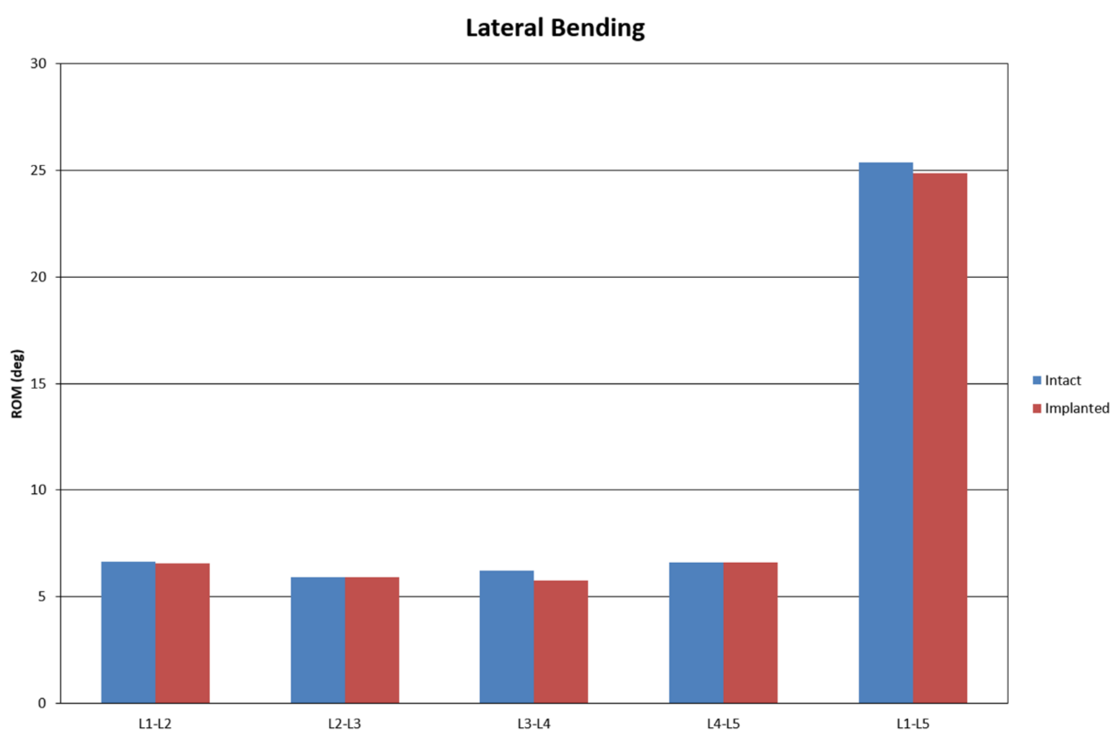

Figure 21: Hybrid lateral bending ROM for intact and implanted model

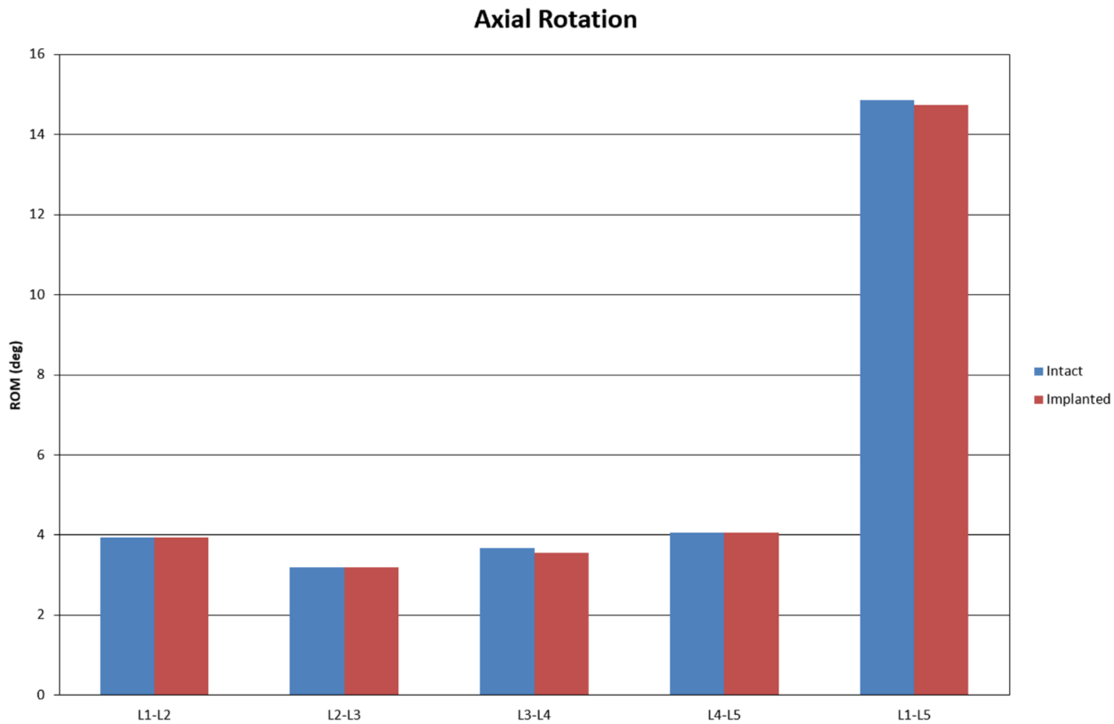

Figure 22: Hybrid axial rotation ROM for intact and implanted model

Facet Loads

Table 3 lists the left and right facet loads at the index and adjacent levels. In extension, a comparison of facet loads at the index and adjacent levels in both models reveals that at the index level in the implanted model, the facet loads decreased significantly—up to 99.9%—relative to the intact model. However, at the superior (L2–L3) and inferior (L4–L5) adjacent levels, the facet loads increased up to 51.9% and up to 60.3%, respectively. At the index level, the facet load changed by up to 22% and 15% in lateral bending and axial rotation, respectively, but it did not change in flexion. At the adjacent level, the change in the facet load was the same—by up to 7%—in flexion, lateral bending, and axial rotation.

Table 3: Comparison of the predicted facet load between the intact and instrumented FE models for the index and the adjacent segments.

FL(N)	Intact		Instrumented	
	Left	Right	Left	Right
L2-L3	151.72	127.13	230.38	184.02
L3-L4	156.99	147.36	11.09	0.06
L4-L5	194.33	120.37	299.92	192.95

Intradiscal Pressure

Table 4 presents the maximum IDP at the index and adjacent levels for both the intact and implanted models. The predicted IDP at the index level in the intact model was 0.98 MPa in extension but it decreased by 52.6% after implantation. In contrast, the predicted IDP at the superior adjacent level in the intact model was 0.87 MPa but it increased significantly by 40% after implantation. Further, the predicted IDP at the inferior adjacent level in the intact model was 0.90 MPa but it increased moderately by 6.6% after implantation. At the index level, the IDP changed by 5% in lateral bending, but it did not change in flexion and axial rotation. At the adjacent level, the IDP was the same as that in the intact model in flexion, lateral bending, and axial rotation.

Table 4: Comparison of the predicted IDP between the intact and instrumented FE models for the index and the adjacent segments

IDP(MPa)	Intact	Instrumented
L2-L3	0.87	1.21
L3-L4	0.98	0.47
L4-L5	0.90	0.96

Stress in Spinous Processes

Figure 23 shows the predicted von Mises stress distribution in spinous processes before and after implantation, in extension. The maximum von Mises stress in the L3 spinous process increased significantly (to 53 MPa) after implantation. Similarly, the maximum predicted von Mises stress in the L-4 spinous process was 48.2 MPa after implantation.

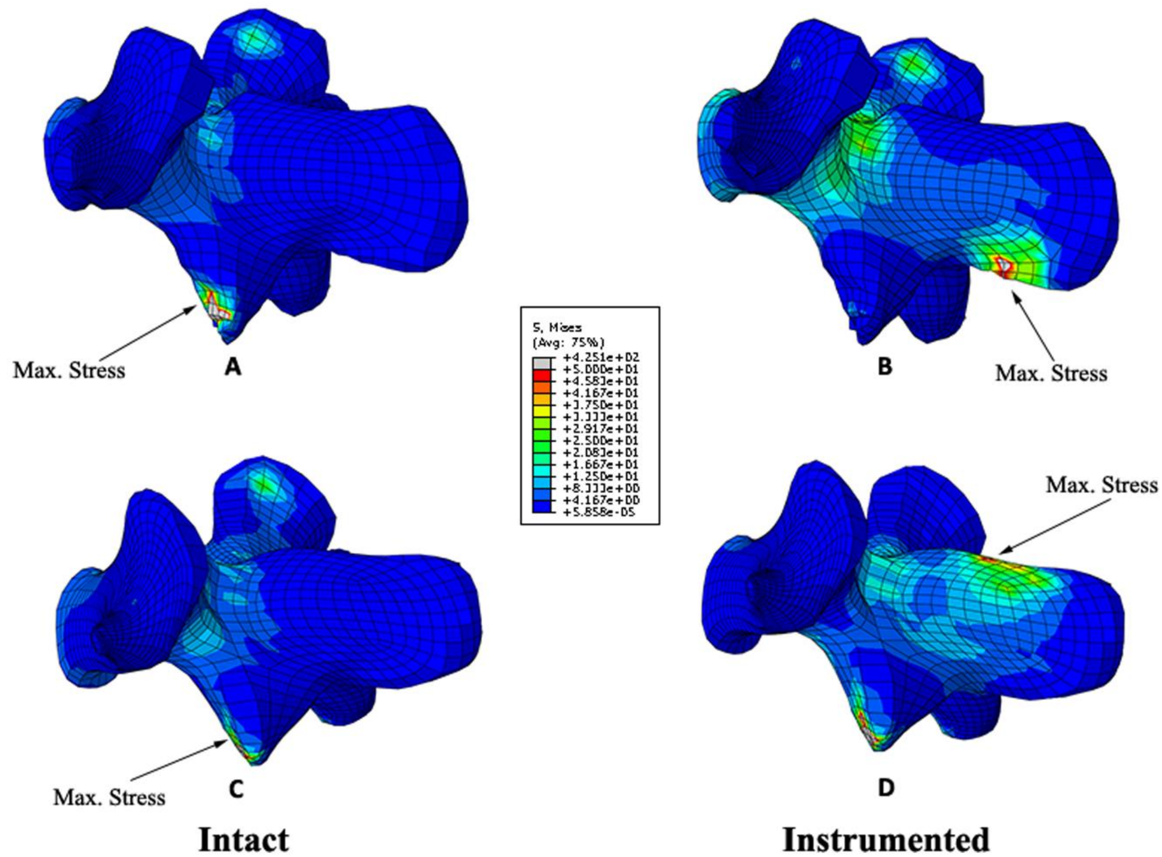

Figure 23: Von Mises stress distribution at the posterior lumbar spine. A: Intact L-3 posterior. B: Implanted L-3 posterior. C: Intact L-4 posterior. D: Implanted L-4 posterior.

4.1.3. Discussion

Interspinous process devices are useful in the treatment of various lumbar spine pathologies. Several studies have investigated the effects of such devices on the biomechanical behavior of the lumbar spine at both the index and adjacent segments. However, none of these studies applied the hybrid protocol to investigate adjacent-segment effects. As suggested by Panjabi et al., [81,82] a hybrid approach gives results that represent the actual scenario in clinical cases following surgical procedures and implantation. In particular, a hybrid testing protocol is appropriate for the biomechanical evaluation of adjacent spinal levels [81]. Studies have shown that the hybrid protocol is more anatomically relevant and can better represent the motion and loads experienced by the spine after surgical procedures and implantation [20,81]. Therefore, we attempted to evaluate the biomechanical effect of ISP devices on adjacent and index segments by using the hybrid protocol, which has rarely been attempted in this field.

The FE model (L1–L5) used in this study was successfully validated in all 3 main planes via a comparison of its results with those from various published in vitro studies. Specifically, the model was validated given the fact that the kinematic data predicted by the FE model in all segments were within the standard deviation or close to the average of the results from in vitro studies.

According to the literature [51,76,83], all commercially available ISP devices affect the biomechanics of the lumbar spine only in extension but not in flexion, lateral bending, and axial rotation. Therefore, we modeled an elliptical cylinder–shaped device with lateral wings that mimicked the X-Stop device and placed it between the L3 and L4 spinous processes of the FE model (L1–L5).

We simulated the implanted model in all motion directions. In general, changes in the ROM, IDP, and facet loads were negligible in directions other than extension, as reported in the literature [76,77]. As expected, the IDP, facet load, and ROM decreased after ISP implantation in extension at the index level.

Our kinematic results at the index level in extension were in agreement with corresponding results in the literature [74,76,77,80]. Specifically, our FE study predicted that the ROM reduced to 0.72° after implantation at the index level in extension, which is similar to Lindsey et al.'s [74] observed reduction of 0.5° ± 0.3° after ISP implantation at the index level in extension. Another study6 reported similar results, that is, a reduction in extension, after ISP implantation in flexion-extension. Although we applied the hybrid protocol, which leads to higher loading (14.5 Nm), the restriction of motion in extension at the implanted level was almost the same as that in the aforementioned studies, owing to the design of ISP devices that makes them restrict motion in extension.

The question then is whether ISP surgery affects the kinematics of adjacent segments. Lindsey et al. [74], who had determined ROM at adjacent levels (L2–L3 and L4–L5) after implantation of the X-Stop ISP device into a cadaveric lumbar spine (L2–L5), reported that the ROM at adjacent segments was not significantly affected in flexion-extension. Similarly, Hartmann et al. [77] reported that there was no significant change in the ROM for all segments (L2–L5) in flexion-extension under a pure moment of 7.5 Nm and follower load of 400 N. However, they reported a significant increase in the ROM for an entire specimen (L2–L5) during lateral bending and rotation after implantation of 4 different ISP devices, and they suggested further investigation of ISP devices for determining adjacent-level effects (ALEs).

In contrast to these findings, our FE model predicted increased motion in the superior and inferior adjacent segments after ISP implantation in extension under hybrid loading (pure moment of 14.5 Nm) and a follower load of 400 N. Although an increase in motion may not lead to adjacent-segment hypermobility due to changes in extension only and perhaps is not clinically significant, it may be useful to investigate the effect of motion changes on other components at adjacent levels, such as facet joints and intervertebral discs.

Further, in this study the facet loads predicted by the FE model for the intact model at the index segment were consistent with those reported in the literature [13]. After implantation of the ISP device, the facet load decreased at the index level in extension. Wiseman et al. [78] reported similar findings: they reported ALEs after implantation and found an increase in the facet load (by 10%) at the superior adjacent level and a decrease in the facet load (by 17%) at the inferior adjacent level. However, they also reported that the changes were not significantly different between the intact and implanted specimens. In contrast to their results, our FE model predicted that the facet load would increase by up to 60% in extension at both the superior and inferior adjacent levels. This contrast in results can be explained as follows. Wiseman et al. [78] placed a pressure-sensitive film in the facet joint to investigate the load values and compared them between the intact and implanted specimens at the adjacent and index segments by using a load control protocol. However, this approach has some drawbacks: a ± 15% error, which was associated with the pressure measurement; variation in the contact area of the pressure sensor; and unsuitability of the load control protocol for adjacent-level investigations. In comparison, the hybrid protocol is more appropriate for evaluating ALEs after implantation of a healthy lumbar FE model. Therefore, our results suggest that after ISP implantation, the adjacent-level facet joint will be affected over the long term and should be subjected to further investigation. At the index level, the facet loads changed by up to 22% and 15% in lateral bending and axial rotation, respectively. These changes were attributed to the wings of the ISP device, which limit motion in these directions. However, the total facet load in the index segment remained similar to that in the intact model, and only the load sharing between the right and left facets changed. In contrast, in extension, the total facet load changed—that is, it decreased.

Interspinous process devices prevent motion in extension and unload the intervertebral disc, resulting in an enlargement of the central canal for the treatment of neurogenic intermittent claudication. As expected, the FE model predicted that the ISP device would release IDP at the index level in extension. This result was in agreement with those in cadaveric studies in the literature [76,79]. However, the FE model predicted that the IDP at the superior adjacent segment (L2–3) would increase by almost 40% after ISP implantation and that this IDP was very close to that in the intact case at the inferior adjacent segment (L4–L5) in extension. Unfortunately, these results disagree with those in a cadaveric study by Swanson et al. [79]. One of the reasons for this disagreement is that Swanson and colleagues performed load control (that is, a flexibility test) instead of displacement control (that is, a hybrid test) for adjacent-level investigations. Another reason, as mentioned in the previous paragraph when discussing the results for facet loads, is that Swanson et al. used a pressure transducer, which may not measure IDP correctly, as suggested by Wilke et al. [76]. Therefore, the efficiency of the intended use of ISP devices may not be correctly interpreted by flexible testing.

Although successful outcomes pertaining to the use of ISP devices in the treatment of lumbar spine diseases have been reported [84,85], a few cases of ISP failure after surgery have been described as well. For example, Miller et al. [86] reported 2 cases of ISP failure in which gradual erosion of the spinous processes occurred because of consistent motion at the spacer-bone interface. Furthermore, Bowers et al. [87] published medical records of complications associated with implantation of the X-Stop device. They reported the fracture of spinous processes in 3 of 13 patients and suggested possible causes of fracture, including the degree of osteoporosis and over-distraction of the interspinous space with an oversized implant. Kim et al. [88] reported a high rate (52%) of spinous process fracture associated with ISP surgery performed in 39 patients at their institution. One of the main reasons for spinous process fracture would be the stress concentration at the bone after ISP implantation. Our FE study drew a clear conclusion in this regard and showed that the stress distribution in spinous processes at the index level changed significantly after implantation. In the intact model, most of the stresses were concentrated at the facet joints. After implantation, however, a greater part of the stress was transferred to the implanted region (Figure 23). Similarly, other studies [80] reported an increase in the load transmitted through spinous processes. Although spinous processes may be strong enough to withstand the stresses after implantation [89], ISP devices may cause gradual erosion at the bone-implant interface under constant stress and motion, thereby increasing the recurrence probability of preoperative symptoms. In addition, the success rate of the outcome of lumbar treatment with an ISP device also depends largely on the bone density8 and overall lumbar scoliosis19 of patients.

Like any other numerical study, this study has certain limitations. Unlike cadaver studies, FE models do not account for the variation in material properties or geometry. Furthermore, some assumptions and simplifications in the model may not represent real values for the human spine. Nevertheless, the predicted data for the intact case are in agreement with the results of cadaver studies.

4.2. Spring Based Pedicle Screw

4.2.1. Method

A study was carried out to determine the biomechanical effect of spring rod based pedicle screw PDS system. Two different designs of spring rod were considered, as shown in Figure 24. Three cases of implanted model were considered to determine load sharing in lumbosacral FE model after instrumentation. All implants were inserted between L4-L5 lumbar segments. The implanted cases were: i) rigid rod fusion (RRF); ii) Titanium spring rod (SR-Ti); and iii) Nitinol spring rod (SR-Ni). Rigid rod and titanium spring rod was given the material property of Titanium alloy with isotropic elastic formulation (Young's modulus: 115 GPa, Poisson's ratio: 0.3). Spring rod was assigned the material property of Nitinol (Titanium and Nickel alloy) with isotropic elastic formulation (Young's modulus: 83 GPa, Poisson's ratio: 0.3).

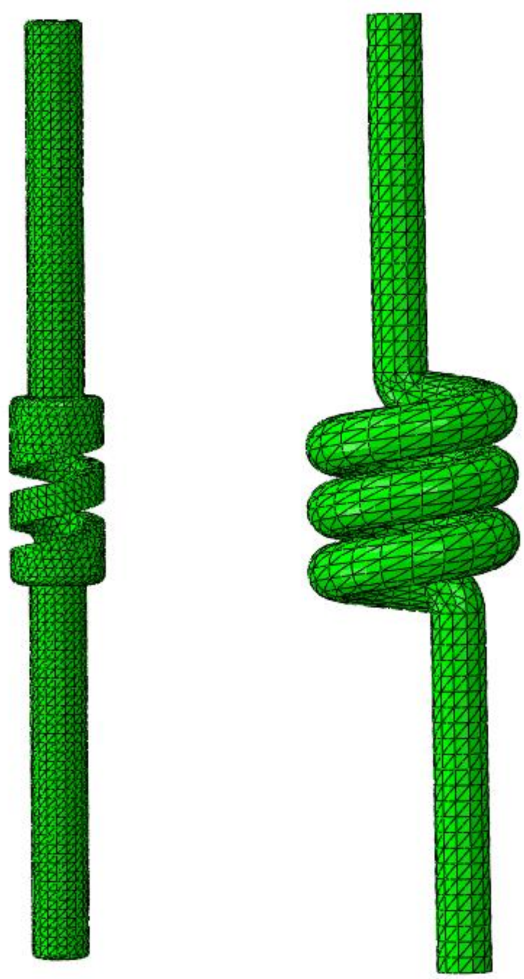

Figure 24: Spring rod with two different models: Titanium (left) and Nitinol (right)

4.2.2. Results

Range of Motion:

ROM was predicted for all four intact and instrumented cases in three loading planes. Figure 25 shows the resulting hybrid ROM for intact and instrumented lumbar spine in extension. The extension ROM values were predicted as 3.22˚ for intact case at index level which decreased to 0.12˚, 0.25˚ and 0.80˚ for RRF, SR-Ti and SR-Ni, respectively. ROM in extension at upper adjacent level was predicted as 3.64˚ for intact which increased to 4.39˚, 4.40˚ and 4.29˚ for RRF, SR-Ti and SR-Ni, respectively. At lower adjacent level, extension motion resulted in ROM of 2.96 which increased to 3.66˚, 3.45˚ and 3.37˚ for RRF, SR-Ti and SR-Ni, respectively. In flexion, the predicted ROM value for intact case at index level was 5.02˚ which decreased to 0.58˚, 0.91˚ and 1.31˚ for RRF, SR-Ti and SR-Ni, respectively (Figure 26). The ROM at adjacent levels in flexion remained within 0.1 after instrumentation in all three cases.

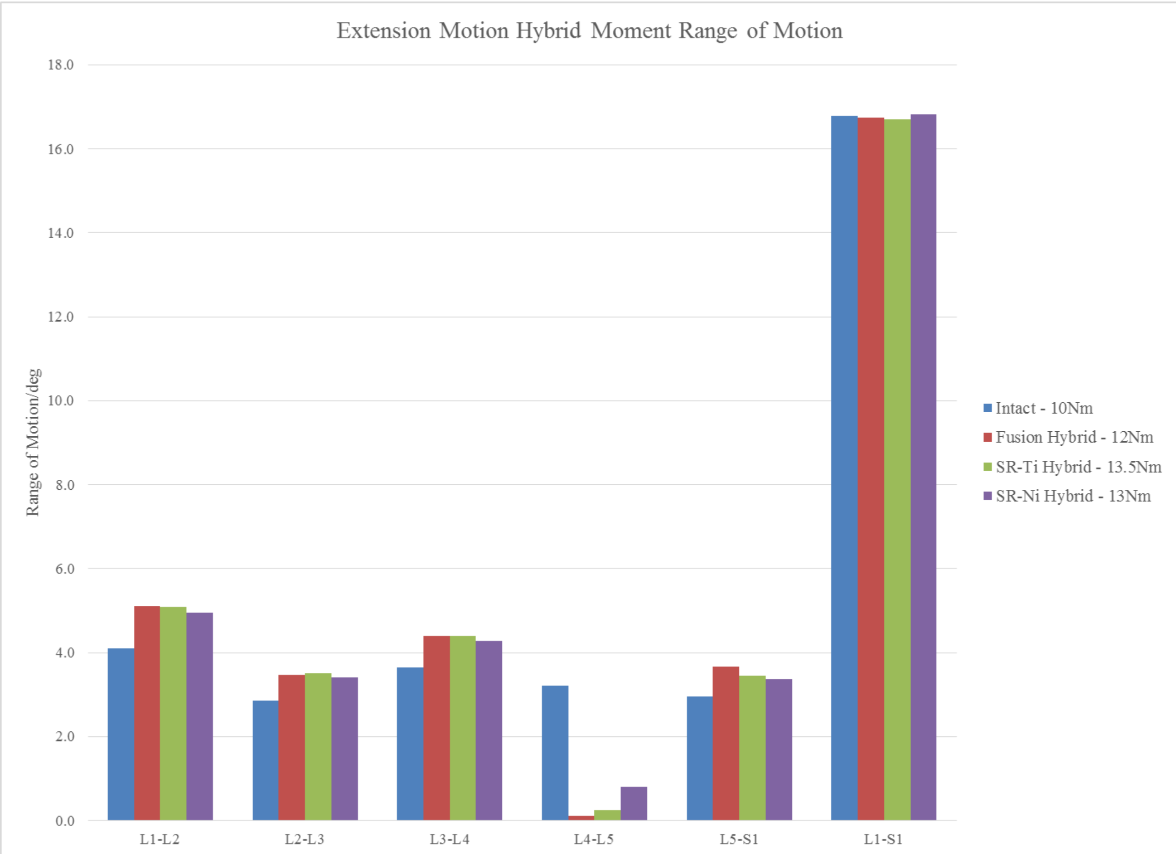

Figure 25: Extension ROM for intact and hybrid instrumented lumbar spine

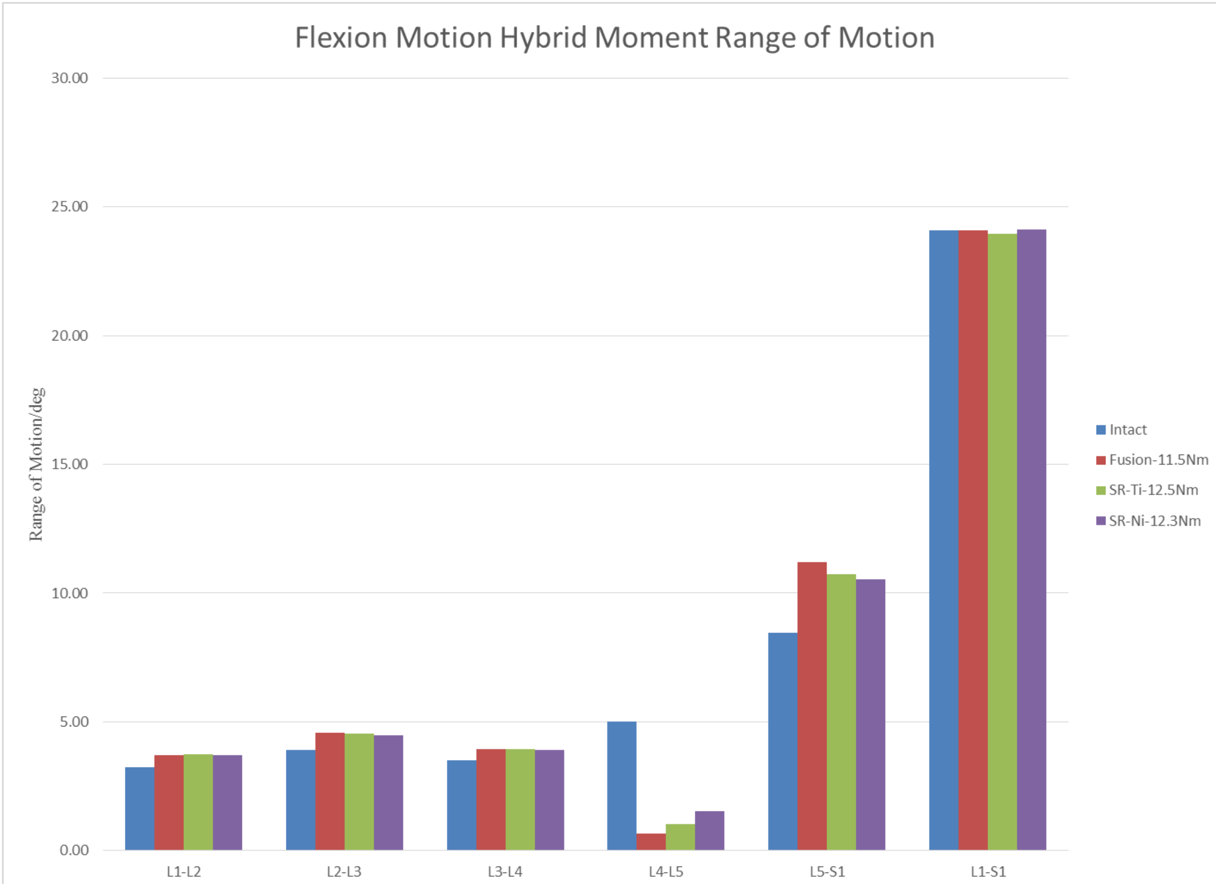

Figure 26: Flexion ROM for intact and hybrid instrumented lumbar spine

ROM for right lateral bending at index level of intact case was predicted as 7.05˚ which decreased to 0.02˚, 0.97˚ and 2.05˚ for RRF, SR-Ti and SR-Ni, respectively (Figure 27). Similarly, for left lateral bending, the ROM at index level was predicted as 6.40˚ for intact which decreased to 0.18˚, 0.81˚ and 1.95˚ after RRF, SR-Ti and SR-Ni, respectively. The adjacent segments for both right and left lateral bending changed less than 0.1 for all three instrumented cases.

ROM for right axial rotation (Figure 28) was predicted as 3.92˚ at index level of intact case. Similarly, ROM for left axial rotation at index level of intact lumbar was predicted as 3.96˚. ROM decreased to 0.16˚, 0.66˚ and 1.07˚ for RRF, SR-Ti and SR-Ni, respectively, for both left and right axial rotation. The adjacent levels had change of less than 0.05˚ after instrumentation of all three types for both left and right axial rotation.

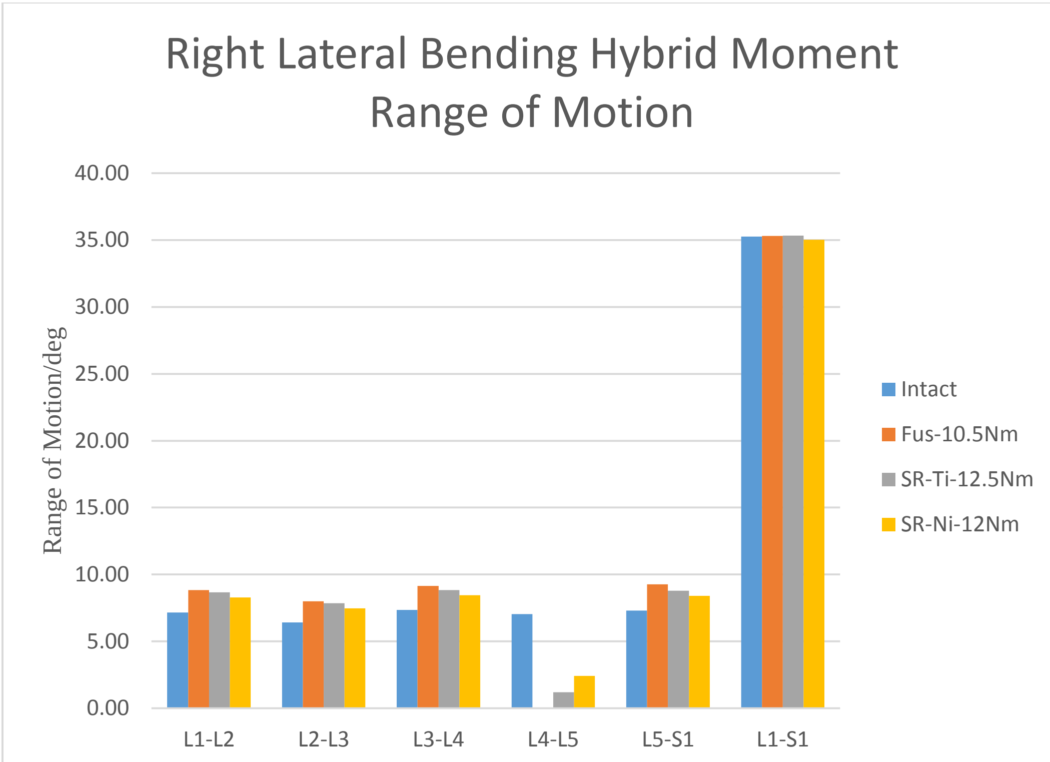

Figure 27: Right Lateral Bending ROM for intact and hybrid instrumented lumbar spine

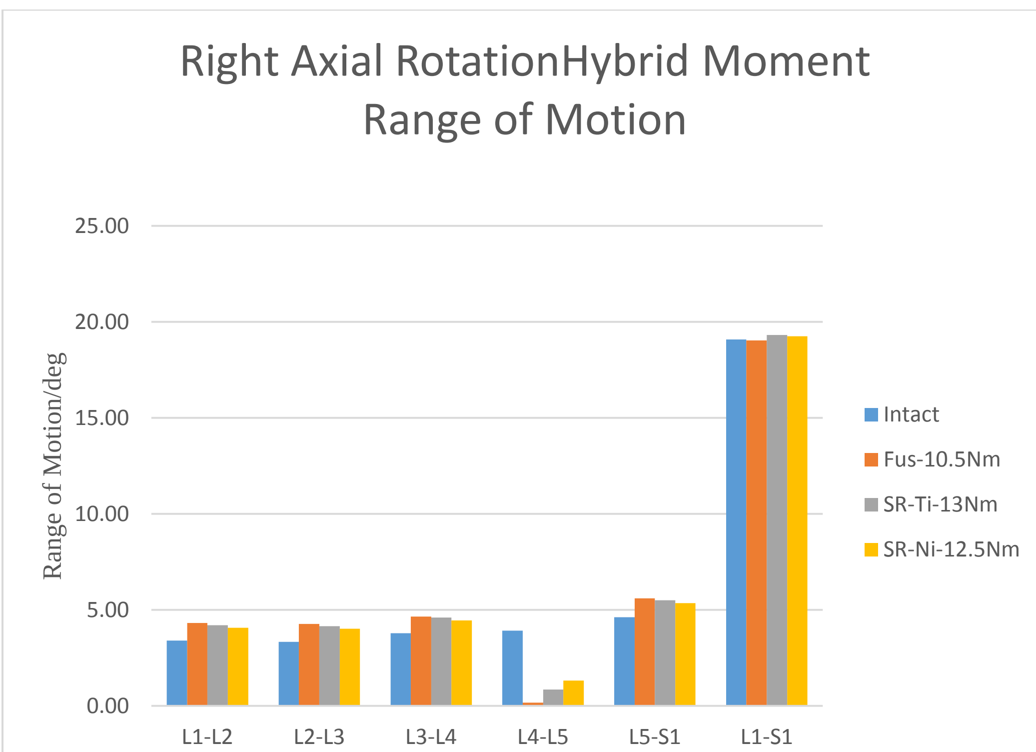

Figure 28: Right Axial Rotation ROM for intact and hybrid instrumented lumbar spine

Intervertebral Disc Pressure:

The maximum pressure in the nucleus of intervertebral disc was predicted at index and adjacent levels. Table 5 shows the predicted IDP for intact and instrumented cases for extension motion where predicted IDP at intact index level was 0.77MPa which decreased to 0.17, 0.21 and 0.31MPa for RRF, SR-Ti and SR-Ni, respectively. In flexion, the IDP for intact case was predicted as 1.39MPa which decreased to 0.90, 1.08 and 1.14MPa after instrumentation with RRF, SR-Ti and SR-Ni, respectively (Table 6). Right lateral bending had predicted IDP of 2.27MPa at index intact level which decreased to 0.83 and 1.12MPa for SR-Ti and SR-Ni, respectively (Table 7). In right axial rotation, the IDP was predicted as 1.15MPa for intact case. The IDP decreased to 0.82 and 0.94MPa after instrumentation with SR-Ti and SR-Ni, respectively (Table 8).

Table 5: IDP for intact and instrumented models after extension hybrid loading

IDP(MPa)	Intact	Fus-12Nm	SR-Ti-13.5Nm	SR-Ni-13Nm
L1-L2	1.15	1.28	1.43	1.37
L2-L3	0.79	0.90	0.93	0.89
L3-L4	0.90	1.02	1.01	1.00
L4-L5	0.77	0.17	0.21	0.31
L5-S1	1.04	1.07	1.21	1.19

Table 6: IDP for intact and instrumented models after flexion hybrid loading

IDP(MPa)	Intact	Fus-11.5Nm	SR-Ti-12.5Nm	SR-Ni-12.3Nm
L1-L2	1.46	1.91	1.64	1.62
L2-L3	1.39	1.70	1.58	1.56
L3-L4	1.30	1.56	1.45	1.44
L4-L5	1.39	0.90	1.08	1.14
L5-S1	2.44	2.77	2.92	2.88

Table 7: IDP for intact and instrumented models after right lateral bending hybrid loading

IDP(MPa)	Intact	Fus-10.5Nm	SR-Ti-12.5Nm	SR-Ni-12Nm
L1-L2	2.33	2.75	2.72	2.65
L2-L3	2.11	2.51	2.47	2.40
L3-L4	2.07	2.46	2.39	2.33
L4-L5	2.27	0.54	0.83	1.12
L5-S1	2.16	2.27	2.43	2.38

Table 8: IDP for intact and instrumented models after right axial rotation hybrid loading

IDP(MPa)	Intact	Fus-10.5Nm	SR-Ti-13Nm	SR-Ni-12.5Nm
L1-L2	1.41	1.85	1.72	1.67
L2-L3	1.40	1.64	1.73	1.68
L3-L4	1.28	1.56	1.52	1.48
L4-L5	1.15	0.53	0.82	0.94
L5-S1	2.12	2.42	2.50	2.44

The effect of instrumentation on the adjacent segment was also predicted. For the superior adjacent segment (L3-L4), instrumentation caused increase in IDP of about 12% in extension for all three instrumentations. In flexion, rigid fusion has highest increase of 20% in IDP where as both spring rods caused increases of around 11% in IDP. In right lateral bending, SR-Ti caused increase in IDP of 15% while SR-Ni instrumentation resulted in 13% increase in IDP at L3-L4. In right axial rotation, an increase in IDP of 19% after SR-Ti instrumentation while an increase of 16% was observed after SR-Ni instrumentation.

For the inferior adjacent segment (L5-S1), instrumentation caused increase in IDP. In extension, an increase of 3%, 16% and 14% in IDP was predicted after instrumentation with RRF, SR-Ti and SR-Ni, respectively. In flexion, an increase of 14%, 20% and 18% in IDP was predicted after instrumentation with RRF, SR-Ti and SR-Ni, respectively. In right lateral bending, after instrumentation with SR-Ti and SR, an increase of 13% and 10% in IDP was predicted, respectively. In right axial rotation, an increase of 18% and 15% in IDP was predicted after SR-Ti and SR-Ni instrumentation, respectively.

Facet Loads (FL):

Total load on facets was predicted at index and adjacent levels of intact and instrumented spines. Table 9-12 shows FL for extension, flexion, right lateral bending and right axial rotation. In extension, intact index level predicted facet load was 320N which decreased to 0.18, 6.76 and 27.27N RRF, SR-Ti and SR-Ni, respectively. Flexion motion had predicted facet load of 70N which decreased to 1.61, 0.5 and 1.47N after RRF, SR-Ti and SR-Ni instrumentation, respectively. In right lateral bending, FL for intact was 87.92N while the instrumentation resulted in predicted facet loads of 8.21 and 16.96N SR-Ti and SR-Ni, respectively. In right axial rotation, the predicted facet loads were 196.76, 7.73 and 20.75N for intact, RRF, SR-Ti and SR-Ni, respectively. In left axial rotation, the predicted facet loads were 208, 0.9, 2.8 and 4.5N for intact, SR-Ti and SR-Ni, respectively. The adjacent levels had change of less than 5% in all instrumentation cases compared to intact case.

Table 9: Facet loads in extension for intact and instrumented models

FL(N)	Intact	Fus-12Nm	SR-Ti-13.5Nm	SR-Ni-13Nm
L1-L2	200.11	273.16	288.99	275.79
L2-L3	283.01	356.43	382.05	368.69
L3-L4	308.78	394.30	418.12	403.30
L4-L5	318.29	0.18	6.76	27.27
L5-S1	319.01	402.90	441.08	425.44

Table 10: Facet loads in flexion for intact and instrumented models

FL(N)	Intact	Fus-11.5Nm	SR-Ti-12.5Nm	SR-Ni-12.3Nm
L1-L2	192.03	239.05	253.63	248.89
L2-L3	119.06	151.50	161.40	158.36
L3-L4	168.08	200.73	217.73	214.27
L4-L5	68.88	1.61	0.50	1.47
L5-S1	0.00	0.00	0.00	0.00

Table 11: Facet loads in lateral bending for intact and instrumented models

FL(N)	Intact	Fus-10.5Nm	SR-Ti-12.5Nm	SR-Ni-12Nm
L1-L2	66.21	90.11	90.97	85.46
L2-L3	31.02	40.58	41.38	39.07
L3-L4	57.86	94.57	90.61	83.62
L4-L5	87.92	1.08	8.21	16.96
L5-S1	138.53	172.90	179.65	171.92

Table 12: Facet loads in right axial rotation for intact and instrumented models

FL(N)	Intact	Fus-10.5Nm	SR-Ti-13Nm	SR-Ni-12.5Nm
L1-L2	156.27	192.71	217.46	207.00
L2-L3	187.46	228.73	255.15	243.54
L3-L4	219.46	260.93	295.58	282.96
L4-L5	196.76	0.77	7.73	20.75
L5-S1	170.49	208.17	234.92	224.41

4.2.3. Discussion

Facet apophyseal joints simulation remained a concern in the prior FE models. Most FE models have symmetrical facet planes [13,43] across mid-sagittal plane. Some studies have used hard frictionless contact with varying Young's modulus and Poisson's ration values [11,18]. Our proposed FE model has asymmetric facet planes about mid-sagittal plane. Similar approach has been taken by some other FE models present in literature [13,17,43] but these models have symmetric facet plane. However, our model contained asymmetrical facet planes which better mimic the original lumbar spine facet joints, and hence, makes the analysis more realistic.

The validated lumbar FE model was used in analysis of pedicle dynamic spring-rod based devices. Two spring-rods were used with different design and material properties. Rigid rod fusion case was taken as control to compare the effectiveness of spring-rod pedicle devices. As opposed to load-control method in numerous previous studies [12,13,90], we employed hybrid loading to investigate the effect of these devices on the biomechanical behavior of lumbosacral spine. According to Panjabi et al. [82], hybrid loading method provides results which are close to real surgical and implanted clinical cases. A detailed study was performed which predicted biomechanical parameters such as range of motion, facet stresses, and intradiscal pressure under hybrid loading. At index level, rigid fusion reduced most of extension motion, followed by titanium spring rod (SR-Ti). Nitinol spring-rod (SR-Ni) was found to be good for restoring motion (up to 24%) in extension plane. These results can be explained by the lower modulus of Nitinol compared with Titanium. Similarly, in axial rotation and lateral bending, spring rods of both types were able to restore greater motion than RRF. This trend has been in accordance with results reported by in vivo study of Kim et al. [56] who concluded that Nitinol based spring rod system is better for dynamic stabilization and reduction of adjacent segment degeneration.

RRF has been in clinical use for decades and for several years, it was the first choice for treating chronic low back pain [91]. However, a number of issues were identified with the rigid fusion. The patients with considerable improvement after fusion were low. Rigid fusion was also a cause of adjacent level effects. RRF has been extensively studied in literature using in vitro and in vivo models. FE model have also been utilized; however, a majority of those computational models were symmetric in nature, which made their analysis less realistic.

CHAPTER 5 Graded Facetectomy

Lumbar facetectomy has been widely accepted as a clinical procedure for spinal stenosis treatment. The physiopathology of spinal stenosis includes bulging of the intervertebral disc, facet thickening, and hypertrophy of the ligamentum flavum [92]. The most common surgical treatment for spinal stenosis involves dorsal decompression, that is, opening up the spinal canal via facetectomy and/or laminectomy. The surgery can either consist of hemifacetectomy or laminectomy and, in each case, it can be either unilateral or bilateral, depending on the extent of the stenosis [70]. A major consequence of the facetectomy is that it increases spinal instability and, subsequently, causes deformation of vertebrae. It would help surgeons to determine the degree of the instability resulting from facetectomy. This will have impact on the decision to perform spinal fusion surgery in such patients.

Several *in vitro*, *in vivo* and FE studies can be found in literature that analyze the effect of facetectomy on the lumbar spine. In an in vitro study, Abumi et al. [93] analyzed lumbar spinal stability by performing unilateral and bilateral medial and total facetectomies. Their results revealed a positive correlation between the extent of facetectomy and the range of motion (ROM) for flexion and axial rotation. Okawa et al. [94] performed a cadaveric study to examine the effect of partial laminectomy and facetectomy on lumbar segmental stability. They carried out cyclic loading tests in compressive and bending directions with unilateral and bilateral facetectomy; their results showed an insignificant effect of facetectomy on flexion and lateral bending. Yue et al. [95] performed *in vitro* and *in vivo* studies and concluded that lumbar instability significantly increased after 50% graded facetectomy. However, such *in vitro* experiments pose several shortcomings. There are variations in bone quality, i.e., the lumbar spine may be diseased, infected by viruses, or may be obtained from elderly individuals with degraded bone [96]. Moreover, cadaver segment studies are not reproducible for multiple experiments.

An alternative biomechanical model for such *in vitro* models is the finite element mesh (FEM) model, which has become a popular method for analyzing lumbar motion segments. A number of FE models have been proposed in literature. Lee and Teo [97] studied the effects of laminectomy and facetectomy on the stability of the L2–L3 lumbar motion segment using the FEM model. For total bilateral laminectomy coupled with facetectomy, they reported an increase in lumbar kinematics leading to lumbar instability. Kiapour et. al [13] performed graded facetectomy on the symmetrical FE lumbar model and reported increase in lumbar motion. Bresnahan et al. [92] performed the graded removal of posterior elements in the FEM model at L3–L4 and L4–L5 for stenosis treatment; with an increase in the removal of posterior elements, they reported an increase in the flexion–extension and axial rotation motions. Open laminectomy was simulated at L4 of the FEM model by Ogden et al. [98]. Their findings showed an increase in motion due to flexion, extension, and axial rotation but no significant changes in lateral bending. Although these early computational models made significant contributions towards lumbar kinematics, they had several limitations. Most of these models were symmetrical [70,97,99], that is, the left and right halves of the lumbar segment were identical along the mid-sagittal plane. In contrast, the real human spine is asymmetric, that is, the left and right halves of each vertebra show considerable anatomical variations; hence, symmetrical models are not adequately realistic.

The aim of the present study was to use an accurate lumbar L1-L5 FE model in analysis of graded facetectomy. The geometry of the proposed model was asymmetric along the mid-sagittal plane, resulting in realistic modeling and analysis of facetectomy. The effect of each surgical modification was determined and compared with published results from *in vitro* and FE studies

5.1. Methods

The validated 3D FE model of lumbar L1-L5 was used in this study. The model is asymmetrical about mid-sagittal plane and includes facet joints and all seven types of ligaments. Material properties were assigned to each part of lumbar based on values available in literature.

5.1.1. Boundary and Loading Conditions

Before simulating the model, the lowermost layer of the L5 vertebra was fixed. A 400-N follower load was applied using connector wire elements. Two wires were placed at each level, each applying a 200-N load. Changes in the ROM with and without the follower load were measured to confirm that the wires passed through the center of rotation at each lumbar segment.

A difference of 0.2° was considered acceptable [82]. The wires were placed such that there was no buckling or bending in the model. The next step involved applying a 10-Nm bending moment to the top surface of the L1 vertebra in each moment plane, that is, flexion, extension, axial rotation (AR; left and right), and lateral bending (LB; left and right). Changes in the ROM were measured for each case and compared with previously reported values [97]. All boundary conditions and loads were kept identical for the intact and injured models.

5.1.2. Destabilized Model

The intact model was modified at the L4–L5 level to create four modified cases, as listed below:

1. 50% unilateral medial facetectomy (UF-50);
2. 75% unilateral medial facetectomy (UF-75);
3. Total left unilateral medial facetectomy (UF-T);
4. Total bilateral facetectomy (BF-T).

In order to remove the facets, the surrounding CL needs to be removed since it encapsulates the facets [70]. Facet removal was initiated from the lower portion of the facet joint for partial removal. The process was continued upwards, towards the upper portion of the facet joint, culminating in complete facet removal. Figure 29 shows the intact L4-L5 facet joint while Figure 30 shows total L4-L5 facet removal.

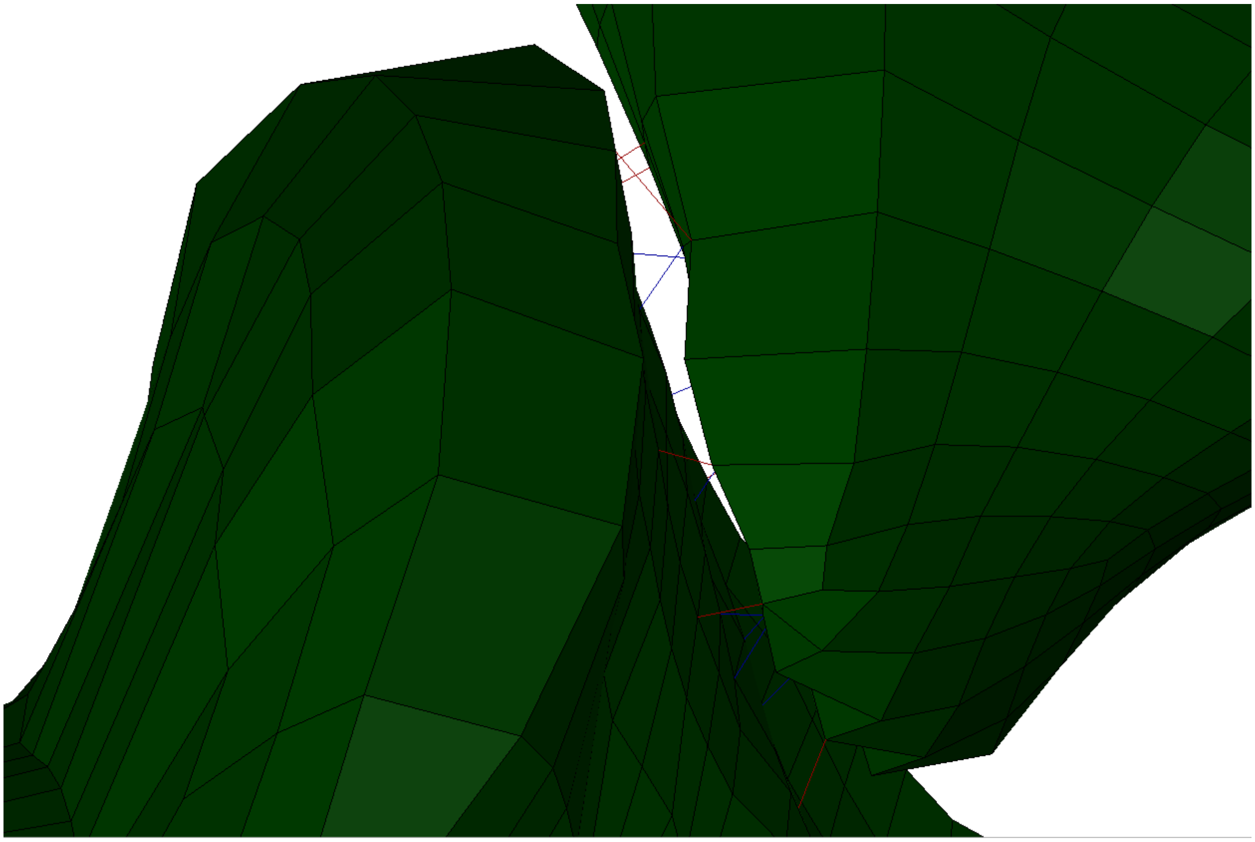

Figure 29: Intact facet joint L4-L5 spinal segment

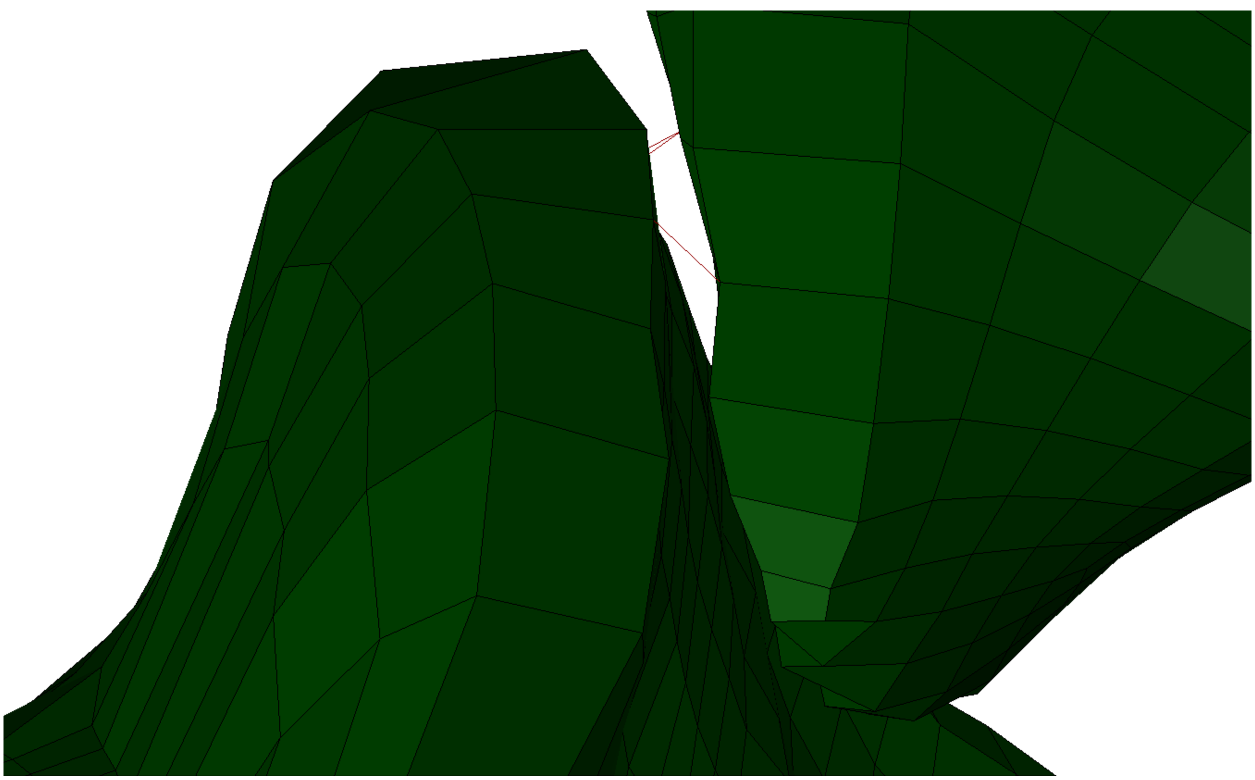

Figure 30: Total facet removal L4-L5 spinal segment

5.2. Results

5.2.1. Range of Motion

The effects of graded facetectomy on the ROM of the lumbar spine were analyzed. Table 13 summarizes the values of the rotation angles for each motion plane for the intact and modified L4–L5 motion segments. In flexion motion, the ROM increased by 14.6% for UF-T at L4–L5. For extension, the three modification levels of UF-50, UF-75, and UF-T resulted in an increase in rotation by 21.2%, 34.9%, and 87.4%, respectively. Similarly, after UF-T, a large increase of 94.5% in the ROM was observed for left AR as compared to the small increase of 10.5% for right AR. Following UF-T, both left and right LB showed a minimal increase, i.e., as less than 8%. The analysis was extended to BF-T, and an increase in rotation of 33.6%, 239%, 120%, 151%, 15.6%, and 12.4% was noted for flexion, extension, left AR, right AR, left LB, and right LB, respectively, in comparison to the values for the intact model.

Table 13: ROM for intact and graded facet removal FE model

L4-L5	Flexion (˚)	Extension (˚)	Left AR (˚)	Right AR (˚)	Left LB (˚)	Right LB (˚)
Intact	5.50	3.45	4.08	3.98	6.62	7.08
50% Left Unilateral	6.17	4.18	4.41	4.40	7.03	7.21
75% Left Unilateral	6.17	4.65	4.77	4.40	7.03	7.28
Total Left Unilateral	6.30	6.47	7.94	4.40	7.04	7.70
Total Bilateral	7.35	11.69	8.99	10.00	7.65	7.96

5.3. Discussion

This study aimed at generating a complete asymmetric FE model of the lumbar spine (L1–L5) using a hexahedral mesh. To ensure realistic results, vertebral and disc asymmetry about the mid-sagittal plane were retained. The asymmetry was a distinct feature of our model, differentiating it from previously proposed symmetrical FE models [70,97,99]. The inherent design simplifications of previously proposed models render their analyses inadequately realistic. The present model was developed using CT scans of the entire spine to ensure accurate geometry of the vertebrae and all the spinal components.

The full lumbar FE model was validated against results from *in vitro* experimental studies to ensure the suitability of the model for further analyses. All three planes of motion were considered during validation. The predicted ROM values in extension closely followed the cadaveric values. However, for flexion, the FE model showed lower ROM than that in *in vitro* studies. Moreover, in lateral bending and axial rotation, large deviations in the ROM were noted, as compared with the *in vitro* values reported by Yamamoto et al. [64]. Some reasons are suggested for this behavior. First, intervertebral discs show variable levels of degradation in cadaver testing [70]. The intervertebral disc plays a significant load-sharing role in lateral bending, axial rotation, and flexion [63]; any degradation in the disc will result in different ROM values. In our FE model, it was not possible to apply varying degrees of degradation to the intervertebral disc; hence, a difference was observed between the *in vitro values* and the predicted values reported here. Second, most *in vitro* studies are performed using cadavers of elderly individuals, who typically have prominent degeneration in the lumbar spine segments [70]. Since the present model was based on a relatively young healthy adult, a difference in the values is possibly inevitable.

In order to investigate the effects of facet on the segmental stability of the lumbar spine, the FE model was subjected to graded facetectomy in four stages at the L4–L5 motion segment [96]. The effect of facet injury on spinal stability varied according to the extent of the injury and the plane of motion. According to the results from the asymmetrical FE lumbar model, for all motion planes, except extension, partial facetectomy did not lead to any substantial changes in the ROM. The tensile stress of the CL maintains vertebral facets under tension and thus limits their ROM. Since the surrounding CL were removed during facetectomy, this led to an increase in the ROM, even with partial facetectomy.

Only the ROM for extension was considerably altered by partial facetectomy, by as much as 87% for total unilateral facetectomy at L4–L5. Furthermore, the ROM for extension increased by 239% when L4–L5 was subjected to total bilateral facetectomy. Such a drastic increase in the ROM for extension has also been reported by Sharma et al. [71], who performed FE analysis for examining the role of vertebral facets. According to their findings, at all moments above 4 Nm, the movement of facet joints is restricted, which provides stiffness to the spinal segment and maintains the motion within physiological limits. In case of any injury to the vertebral facets, the extension motion becomes abnormally high in the case of large moments. Similarly, Kiapour et al. [99] carried out an FE study to analyze the effects of facet removal. Their results showed an increase of 222% in the ROM for extension with total unilateral facetectomy. However, they did not comment on the status of the CL during facet removal; further, their analysis did not consider a complete lumbar model and the asymmetry in lumbar motion segments was not retained.

Similarly, for axial rotation, the present results showed a considerable increase in the ROM following unilateral and bilateral total facetectomy. Abumi et al. [93] performed an *in vitro* facetectomy study and concluded that the ROM increased significantly for axial rotation, depending on the extent of facet injury. Moreover, they suggested that with unilateral total facetectomy, the increase in ROM for axial rotation occurred in the contralateral direction. The present findings also show similar results for axial rotation.

In contrast, in the case of lateral bending, the predicted change was less than 15%, even after total bilateral facetectomy. Therefore, facetectomy to any extent, i.e., partial or complete, does not appear to have any specific effect on the ROM of the lumbar spine in lateral bending. Several other studies have shown similar results [70,93].

A distinctive geometric feature of our model was the asymmetry of the vertebral facet planes around the mid-sagittal plane, unlike previously proposed models [70,97,99]. This asymmetry led to coupled motion, particularly in the extension plane of motion, as described previously [73]. The addition of coupled motion is significant in future studies, such as those concerning the implantation of dynamic devices in the lumbar motion segment. In these scenarios, coupled motion can have significant effect on the motion of the lumbar spine in a particular motion plane.

CHAPTER 6 Whiplash Injury Study Using Imaging

6.1. Introduction

The aim of this study was to determine the effect of headrest material on whiplash injury using the HIII 50th Percentile Anthropomorphic Test Dummy (ATD). The mechanical setup consisted of dummy mounted over a sled which was given rear-impact pulse using hydraulic actuator. The sled and corresponding rail frame were made from aluminum. A marine rope was attached on the back side of sled and wound over a shaft which rotated freely initially. A hydraulic linear actuator was used to give rear-impact low speed pulse to sled. The hydraulic linear actuator consisted of direct-operated servo valves with response time of around 5ms. The highest acceleration produced in the set up was 15g under 15 seconds for whiplash study. A mechanical switch was placed beneath sled which was released when sled moved, subsequently opening the electromagnetic valve and moving air into the pneumatic brake, causing shaft to stop, resulting in rope to go taut and sled to stop. Sensor placement was done as suggested in literature. Accelerometers were placed on the sled, and head and sternum of the dummy, while load cells were placed inside the neck of the dummy. The accelerometer data was recorded through DAC and processed in MATLAB using low pass Butterworth filter to remove high frequency noise.

6.2. Methods & Results:

A high frame rate camera of 1 KHz was used to record the motion for its entire duration. The dummy had visual trackers on head and upper arm which were subsequently tracked in image processing software, ProAnalyst®. Two headrests were used in the analysis: normal car headrest and a new, softer headrest. Three rear impact accelerations were tested in this study: 8.5g, 9.2g, and 11.5g. The tracked points on head and upper arm (torso) were used to determine the angle profile of head-torso. Figures 31-33 show the corresponding angle graph for three accelerations using both types of headrests. Additionally, the time when head impact with headrest occurred and the time during which head remained on headrest before moving forward were determined from tracked data points. For 11.5g rear impact pulse, the impact angle was 75˚ for both headrest types. However, the change in the angle was 11˚ and 18˚, respectively, for normal and improved headrests. The head remained in contact with the headrest for 28ms and 38ms, respectively, for normal and improved headrests. The softer headrest allowed for greater extension of upper cervical spine and, hence, reduced the risk of whiplash injury in cervical spine. Moreover, head remained in contact with softer headrest for longer time which reduced the force in neck, as shown by the load cells.

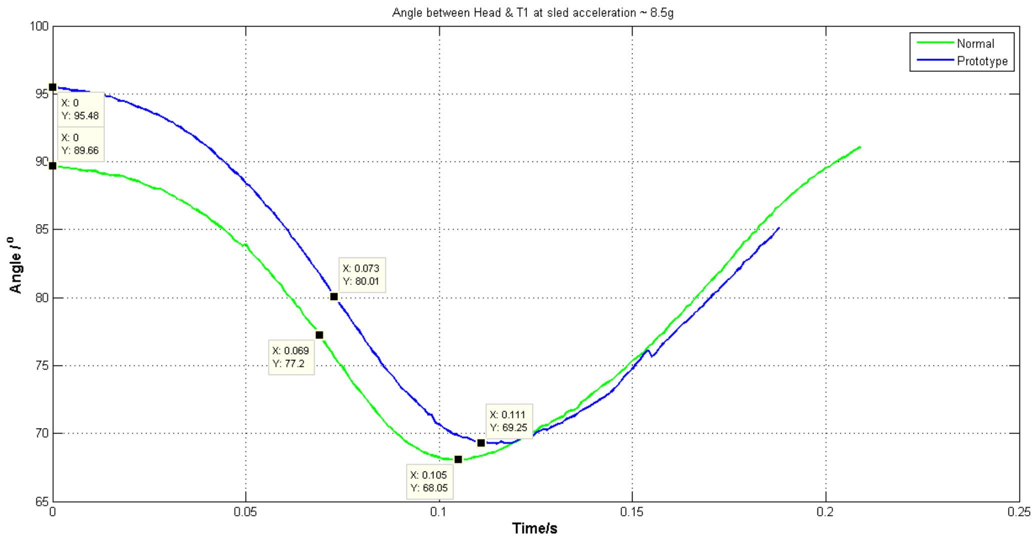

Figure 31: Angle between Head and T1 at sled acceleration of 8.5g

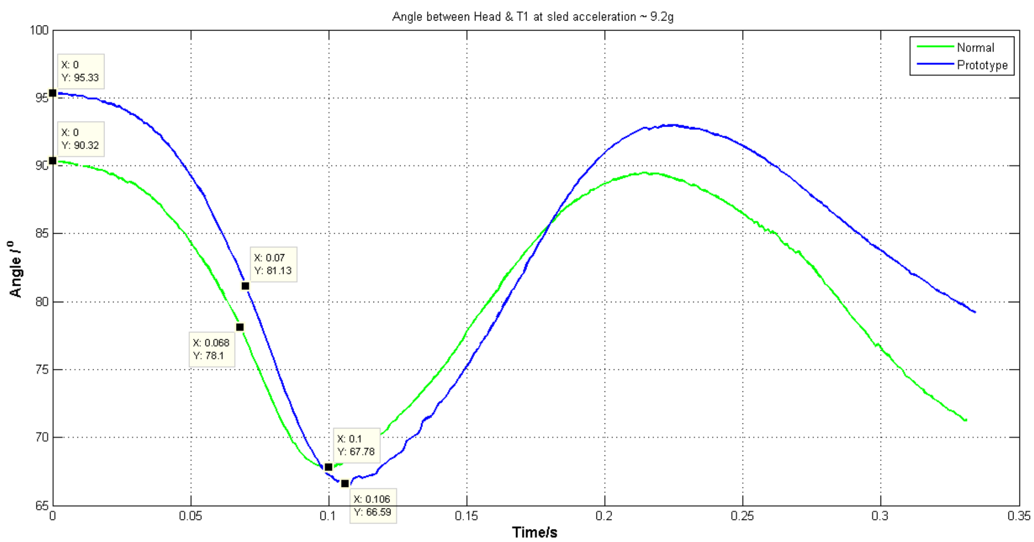

Figure 32: Angle between Head and T1 at sled acceleration of 9.2g

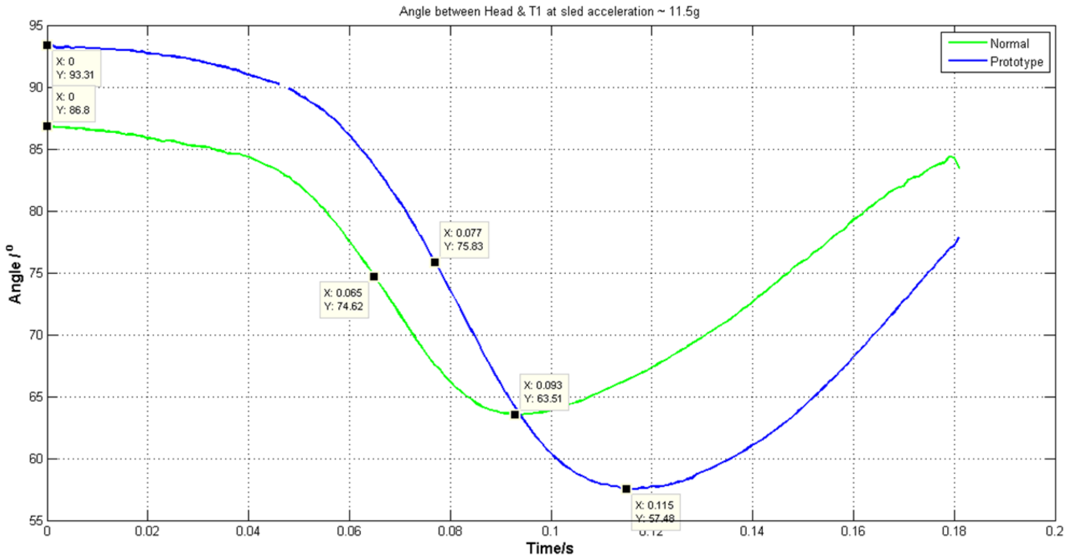

Figure 33: Angle between Head and T1 at sled acceleration of 11.5g

CHAPTER 7 Thoracic FE Model

7.1. Methods

Thoracic spine FE model was generated similar to lumbar FE model. T8-T9 segment was meshed using multi-block method. Hexahedral mesh was created for vertebral body and intervertebral disc. Ligaments were modelled using 2D truss elements while facet joints were simulated using unidirectional gap elements. Material properties were assigned according to the values given in Table 2.

A study was carried out to determine range of motion (ROM) of intact and instrumented thoracic T8-T9 spine. The instrumentation was done using a posterior stabilization system where the trajectory of the screws varied [100]. Figure 34 shows pedicle screw trajectory parallel to pedicle (anatomic trajectory) while Figure 35 shows pedicle screw trajectory parallel to end plates (straight-forward trajectory).

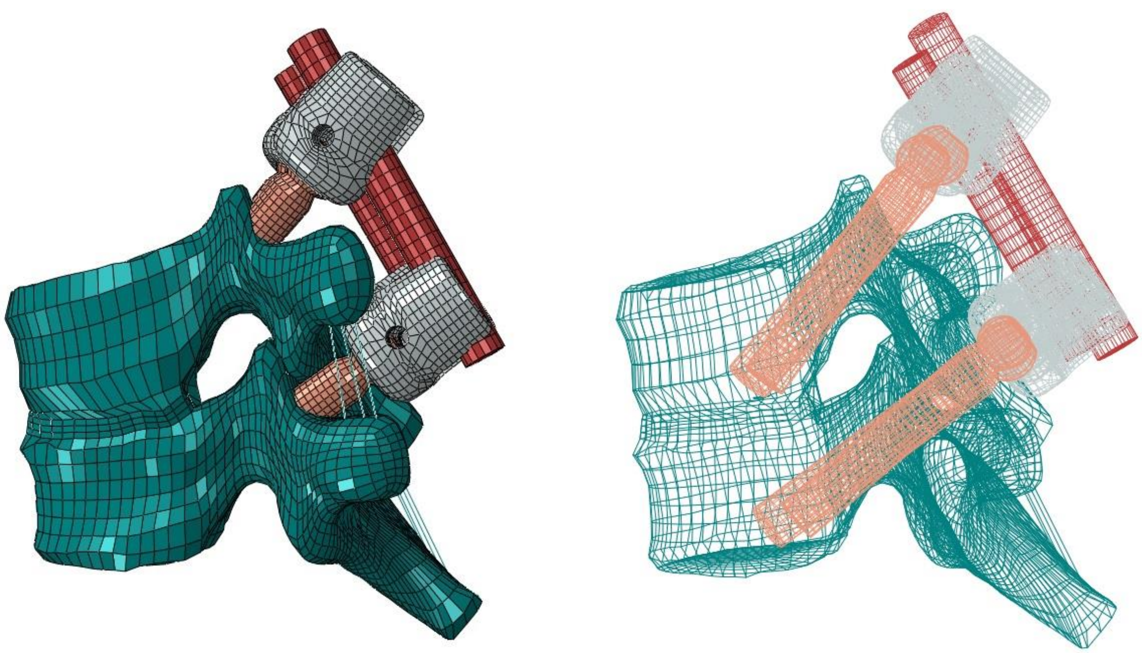

Figure 34: Anatomic trajectory of the screw

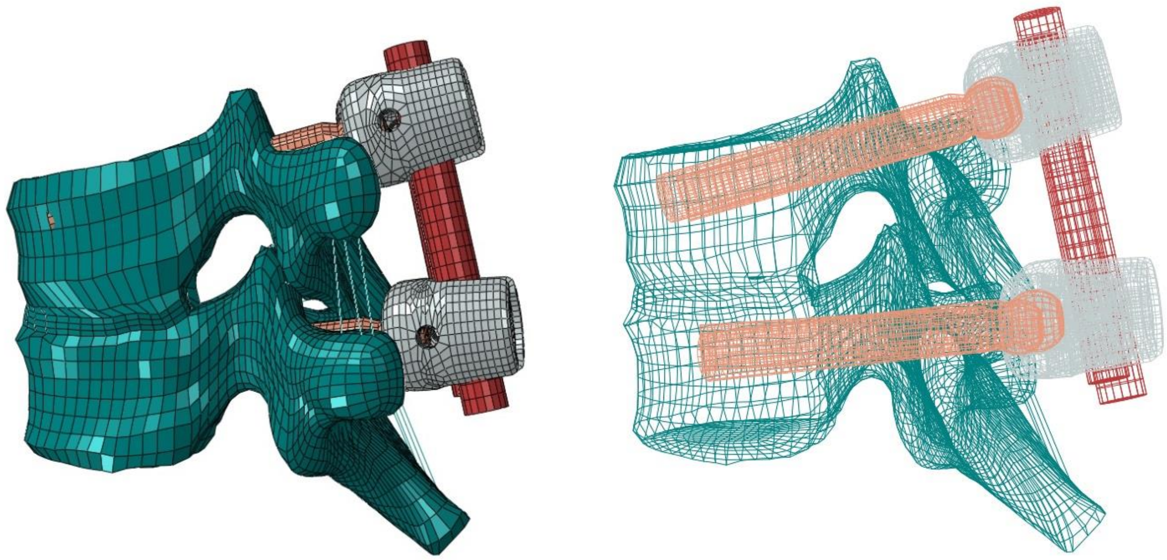

Figure 35: Straight-forward trajectory of the screw

The inferior surface of T9 was fixed, a 10Nm bending moment was applied to the superior surface of the T8 vertebra in the intact spine, and the segmental and overall range of motion was obtained in flexion (Flex), extension (Ext), lateral bending (LB) and axial rotation (AR). Follower load concept was used to apply 400 N as the body weight in each segment.

7.2. Results

Table 14: Range of Motion for intact and intact with instrumented FE thoracic spine

	Flex (º)	Ext (º)	RLB (º)	RAR (º)
Intact	3.2349	3.3013	3.2967	4.1376
AN	3.8944	3.9982	2.7434	2.8988
SN	3.4941	3.6017	4.8082	3.7398

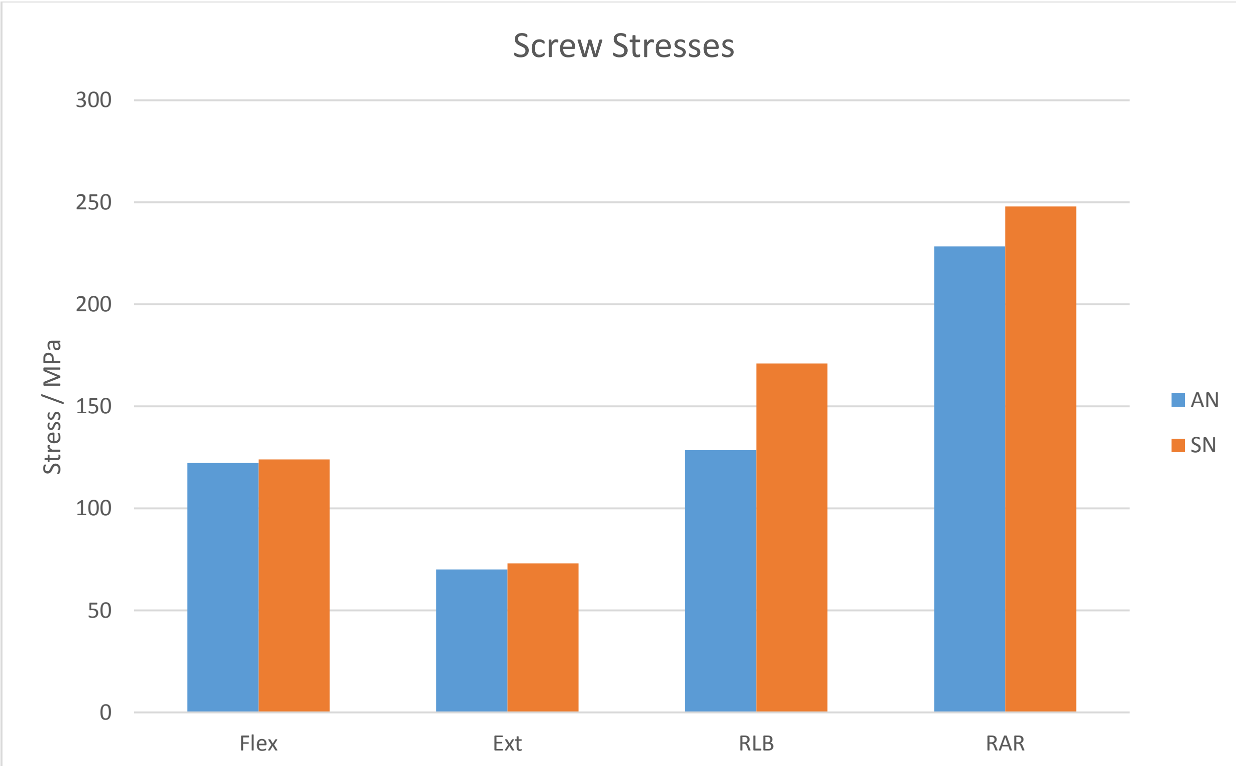

Figure 36: Max von Mises stress on the screw tails

Trajectory of the pedicle screw had a similar effect on the ROM of the treated segment (T8-T9) in axial rotation. The difference between the both techniques was negligible. However, both techniques showed different stress respond under physiological loadings. In Flex, The maximum stress was decreased by 1.4% when pedicle screws were parallel to pedicle. In Ext, the maximum stress was decreased by 4% when pedicle screws were parallel to pedicle. In LB and AR, FE analysis showed decrease in stress by 25% and 8%, respectively, when pedicle screws were parallel to pedicle.

Conclusion

The main objective of this thesis was to develop an accurate finite element model of the complete lumbosacral spine and subsequently, use it for dynamic stabilization device analysis. The model was generated using a novel multi-bloc technique where nodes were placed on the surfaces extracted from CT scans. Hexahedral mesh was generated on the bony structure and intervertebral disc according to node placement. The model was completed by adding 2D truss elements in place of ligaments and adding GAPUNI elements as facet joints. The model was validated against cadaver studies and found to be in good agreement. L1-S1 model was utilized in PDS system analysis of an ISP device and 2 types of spring rods using hybrid loading. It was found that ISP device was not much effective in preventing adjacent segment degeneration. Spring rod made of Nitinol alloy was found to restore more motion than Titanium based spring rod.

Some other studies were carried out such as graded facetectomy, whiplash injury study using image analysis, and thoracic spine pedicle screw trajectory. Graded facetectomy ranged from 50% unilateral facet removal to total bilateral facet removal. It was found that only total facet removal has significant effect on range of motion in extension plane.

References

[1] Miura T, Panjabi MM, Cripton PA, 2002. A method to simulate in vivo cervical spine kinematics using in vitro compressive preload. Spine. 27 (1), 43-48

[2] Goel VK, Mehta A, Jangra J, Faizan A, Kiapour A, Hoy RW, Fauth AR, 2007. Anatomic facet replacement system (AFRS) restoration of lumbar segment mechanics to intact: a finite element study and in vitro cadaver investigation. SAS journal. 1 (1), 46-54

[3] Trautwein FT, Lowery GL, Wharton ND, Hipp JA, Chomiak RJ, 2010. Determination of the in vivo posterior loading environment of the Coflex interlaminar-interspinous implant. The Spine Journal. 10 (3), 244-251

[4] Deng Y-C, 1989. Anthropomorphic dummy neck modeling and injury considerations. Accident Analysis & Prevention. 21 (1), 85-100

[5] Jakobsson L, Lundell B, Norin H, Isaksson-Hellman I, 2000. WHIPS–Volvo's whiplash protection study. Accident Analysis & Prevention. 32 (2), 307-319

[6] Viano DC, Olsen S, 2001. The effectiveness of active head restraint in preventing whiplash. Journal of Trauma and Acute Care Surgery. 51 (5), 959-969

[7] Guan Y, Yoganandan N, Zhang J, Pintar FA, Cusick JF, Wolfla CE, Maiman DJ, 2006. Validation of a clinical finite element model of the human lumbosacral spine. Medical and Biological Engineering and Computing. 44 (8), 633-641

[8] Zhang QH, Teo EC, 2008. Finite element application in implant research for treatment of lumbar degenerative disc disease. Medical engineering & physics. 30 (10), 1246-1256

[9] Schmidt H, Galbusera F, Rohlmann A, Shirazi-Adl A, 2013. What have we learned from finite element model studies of lumbar intervertebral discs in the past four decades? Journal of biomechanics. 46 (14), 2342-2355

[10] Erbulut D, Zafarparandeh I, Lazoglu I, Ozer A, 2014. Application of an asymmetric finite element model of the C2-T1 cervical spine for evaluating the role of soft tissues in stability. Medical engineering & physics. 36 (7), 915-921

[11] Park WM, Kim K, Kim YH, 2013. Effects of degenerated intervertebral discs on intersegmental rotations, intradiscal pressures, and facet joint forces of the whole lumbar spine. Computers in biology and medicine. 43 (9), 1234-1240

[12] Liu C-L, Zhong Z-C, Hsu H-W, Shih S-L, Wang S-T, Hung C, Chen C-S, 2011. Effect of the cord pretension of the Dynesys dynamic stabilisation system on the biomechanics of the lumbar spine: a finite element analysis. European Spine Journal. 20 (11), 1850-1858

[13] Kiapour A, Ambati D, Hoy RW, Goel VK, 2012. Effect of graded facetectomy on biomechanics of Dynesys dynamic stabilization system. Spine. 37 (10), E581-E589

[14] Ayturk UM, Puttlitz CM, 2011. Parametric convergence sensitivity and validation of a finite element model of the human lumbar spine. Computer methods in biomechanics and biomedical engineering. 14 (8), 695-705

[15] Little JP, De Visser H, Pearcy MJ, Adam CJ, 2008. Are coupled rotations in the lumbar spine largely due to the osseo-ligamentous anatomy?—a modeling study. Computer methods in biomechanics and biomedical engineering. 11 (1), 95-103

[16] Schmidt H, Galbusera F, Rohlmann A, Zander T, Wilke H-J, 2012. Effect of multilevel lumbar disc arthroplasty on spine kinematics and facet joint loads in flexion and extension: a finite element analysis. European Spine Journal. 21 (5), 663-674

[17] Shirazi-Adl A, 1994. Biomechanics of the lumbar spine in sagittal/lateral moments. Spine. 19 (21), 2407-2414

[18] Schmidt H, Heuer F, Simon U, Kettler A, Rohlmann A, Claes L, Wilke H-J, 2006. Application of a new calibration method for a three-dimensional finite element model of a human lumbar annulus fibrosus. Clinical Biomechanics. 21 (4), 337-344
[19] Lee K-K, Tian-Xia Q, Teo E-C, 2002. 3-D finite element modeling of lumbar spine (L2/L3) using digitizer. International Journal of Information Technology. 8 (2), 1-9
[20] Goel VK, Grauer JN, Patel TC, Biyani A, Sairyo K, Vishnubhotla S, Matyas A, Cowgill I, Shaw M, Long R, 2005. Effects of charite artificial disc on the implanted and adjacent spinal segments mechanics using a hybrid testing protocol. Spine. 30 (24), 2755-2764
[21] Fice JB, Cronin DS, 2012. Investigation of whiplash injuries in the upper cervical spine using a detailed neck model. Journal of biomechanics. 45 (6), 1098-1102
[22] Leone A, Guglielmi G, Cassar-Pullicino VN, Bonomo L, 2007. Lumbar Intervertebral Instability: A Review. Radiology. 245 (1), 62-77
[23] Gray H (1918) Anatomy of the human body. Lea & Febiger,
[24] Pope MH, 1989. Biomechanics of the lumbar spine. Annals of medicine. 21 (5), 347-351
[25] Panjabi M, White A, 1990. Physical properties and functional biomechanics of the spine. Clinical biomechanics of the spine. 2, 1-83
[26] Adams P, Eyre D, Muir H, 1977. Biochemical aspects of development and ageing of human lumbar intervertebral discs. Rheumatology. 16 (1), 22-29
[27] Beattie P, 1996. The relationship between symptoms and abnormal magnetic resonance images of lumbar intervertebral disks. Physical therapy. 76 (6), 601-608
[28] Raj PP, 2008. Intervertebral Disc: Anatomy-Physiology-Pathophysiology-Treatment. Pain Practice. 8 (1), 18-44
[29] Arutynow A, 1962. Basic problems of the pathology and surgical treatment of prolapsed intervertebral discs. Vopr Neirokhir. 4, 21-24
[30] Roaf R, 1960. A study of the mechanics of spinal injuries. Journal of Bone & Joint Surgery, British Volume. 42 (4), 810-823
[31] Evans J, Nachemson A, 1968. Some mechanical properties of the third lumbar interlaminar ligament. J Biomech. 1, 211-220
[32] Chazal J, Tanguy A, Bourges M, Gaurel G, Escande G, Guillot M, Vanneuville G, 1985. Biomechanical properties of spinal ligaments and a histological study of the supraspinal ligament in traction. Journal of biomechanics. 18 (3), 167-176
[33] Panjabi M, White Ar, Johnson R, 1975. Cervical spine mechanics as a function of transection of components. Journal of biomechanics. 8 (5), 327-336
[34] Prasad P, King A, Ewing C, 1974. The role of articular facets during+ Gz acceleration. Journal of Applied Mechanics. 41 (2), 321-326
[35] Netter F (2006) Atlas of human anatomy 4 th ed. Philadelphia, PA: Saunders.
[36] Ahmed AM, Duncan NA, Burke DL, 1990. The effect of facet geometry on the axial torque-rotation response of lumbar motion segments. Spine. 15 (5), 391-401
[37] Nachemson AL, Schultz AB, Berkson MH, 1979. Mechanical Properties of Human Lumbar Spine Motion Segments: Influences of Age, Sex, Disc Level, and Degeneration. Spine. 4 (1), 1-8
[38] Fiorini GT, McCammond D, 1976. Forces on lumbo-vertebral facets. Annals of biomedical engineering. 4 (4), 354-363
[39] Natarajan RN, Andersson GB, 1999. The influence of lumbar disc height and cross-sectional area on the mechanical response of the disc to physiologic loading. Spine. 24 (18), 1873
[40] Niemeyer F, Wilke H-J, Schmidt H, 2012. Geometry strongly influences the response of numerical models of the lumbar spine—a probabilistic finite element analysis. Journal of biomechanics. 45 (8), 1414-1423

[41] Zander T, Rohlmann A, Bergmann G, 2004. Influence of ligament stiffness on the mechanical behavior of a functional spinal unit. Journal of biomechanics. 37 (7), 1107-1111

[42] Wilke H-J, Neef P, Hinz B, Seidel H, Claes L, 2001. Intradiscal pressure together with anthropometric data–a data set for the validation of models. Clinical Biomechanics. 16, S111-S126

[43] Zander T, Rohlmann A, Bergmann G, 2009. Influence of different artificial disc kinematics on spine biomechanics. Clinical biomechanics. 24 (2), 135-142

[44] Dreischarf M, Zander T, Shirazi-Adl A, Puttlitz C, Adam C, Chen C, Goel V, Kiapour A, Kim Y, Labus K, 2014. Comparison of eight published static finite element models of the intact lumbar spine: Predictive power of models improves when combined together. Journal of biomechanics. 47 (8), 1757-1766

[45] Chou W-Y, Hsu C-J, Chang W-N, Wong C-Y, 2002. Adjacent segment degeneration after lumbar spinal posterolateral fusion with instrumentation in elderly patients. Archives of orthopaedic and trauma surgery. 122 (1), 39-43

[46] Etebar S, Cahill DW, 1999. Risk factors for adjacent-segment failure following lumbar fixation with rigid instrumentation for degenerative instability. Journal of Neurosurgery: Spine. 90 (2), 163-169

[47] Bono CM, Kadaba M, Vaccaro AR, 2009. Posterior pedicle fixation-based dynamic stabilization devices for the treatment of degenerative diseases of the lumbar spine. Journal of spinal disorders & techniques. 22 (5), 376-383

[48] Sengupta DK, 2004. Dynamic stabilization devices in the treatment of low back pain. Orthopedic Clinics of North America. 35 (1), 43-56

[49] Nockels RP, 2005. Dynamic stabilization in the surgical management of painful lumbar spinal disorders. Spine. 30 (16S), S68-S72

[50] Schmoelz W, Huber J, Nydegger T, Claes L, Wilke H, 2003. Dynamic stabilization of the lumbar spine and its effects on adjacent segments: an in vitro experiment. Journal of spinal disorders & techniques. 16 (4), 418-423

[51] Bono CM, Vaccaro AR, 2007. Interspinous process devices in the lumbar spine. Journal of spinal disorders & techniques. 20 (3), 255-261

[52] Erbulut D, Zafarparandeh I, Ozer A, Goel V, 2012. Biomechanics of posterior dynamic stabilization systems. Advances in orthopedics. 2013, 451956-451956

[53] Erbulut DU, Zafarparandeh I, Hassan CR, Lazoglu I, Ozer AF, 2015. Determination of the biomechanical effect of an interspinous process device on implanted and adjacent lumbar spinal segments using a hybrid testing protocol: a finite-element study. Journal of Neurosurgery: Spine. 1-9

[54] Sangiorgio SN, Sheikh H, Borkowski SL, Khoo L, Warren CR, Ebramzadeh E, 2011. Comparison of three posterior dynamic stabilization devices. Spine. 36 (19), E1251-E1258

[55] Kondrashov DG, Hannibal M, Hsu KY, Zucherman JF, 2006. Interspinous process decompression with the X-STOP device for lumbar spinal stenosis: a 4-year follow-up study. Journal of spinal disorders & techniques. 19 (5), 323-327

[56] Kim Y-S, Zhang H-Y, Moon B-J, Park K-W, Ji K-Y, Lee W-C, Oh K-S, Ryu G-U, Kim DH, 2006. Nitinol spring rod dynamic stabilization system and Nitinol memory loops in surgical treatment for lumbar disc disorders: short-term follow up. Neurosurgical focus. 22 (1), E10-E10

[57] Cho BY, Murovic J, Park KW, Park J, 2010. Lumbar disc rehydration postimplantation of a posterior dynamic stabilization system: case report. Journal of Neurosurgery: Spine. 13 (5), 576-580

[58] Hassan CR, Zafarparandeh I, Erbulut DU, Load Sharing in L4-L5 Spinal Motion Segment Using an Asymmetrical Finite Element Model.

[59] Kallemeyn NA, Tadepalli SC, Shivanna KH, Grosland NM, 2009. An interactive multiblock approach to meshing the spine. Computer methods and programs in biomedicine. 95 (3), 227-235
[60] Erbulut DU, Kiapour A, Oktenoglu T, Ozer AF, Goel VK, 2014. A Computational Biomechanical Investigation of Posterior Dynamic Instrumentation: Combination of Dynamic Rod and Hinged (Dynamic) Screw. Journal of biomechanical engineering. 136 (5), 051007
[61] Niosi CA, Zhu QA, Wilson DC, Keynan O, Wilson DR, Oxland TR, 2006. Biomechanical characterization of the three-dimensional kinematic behaviour of the Dynesys dynamic stabilization system: an in vitro study. European Spine Journal. 15 (6), 913-922
[62] Schilling C, Krüger S, Grupp TM, Duda GN, Blömer W, Rohlmann A, 2011. The effect of design parameters of dynamic pedicle screw systems on kinematics and load bearing: an in vitro study. European Spine Journal. 20 (2), 297-307
[63] Schmoelz W, Huber JF, Nydegger T, Claes L, Wilke HJ, 2003. Dynamic stabilization of the lumbar spine and its effects on adjacent segments: an in vitro experiment. Journal of spinal disorders & techniques. 16 (4), 418-423
[64] Yamamoto I, Panjabi MM, Crisco T, Oxland TOM, 1989. Three-dimensional movements of the whole lumbar spine and lumbosacral joint. Spine. 14 (11), 1256-1260
[65] Yamamoto I, Panjabi MM, Crisco T, Oxland T, 1989. Three-Dimensional Movements of the Whole Lumbar Spine and Lumbosacral Joint. Spine. 14 (11), 1256-1260
[66] Schmoelz W, Huber JF, Nydegger T, Claes L, Wilke HJ, 2003. Dynamic Stabilization of the Lumbar Spine and Its Effects onAdjacent Segments? an in vitro experiment. Journal of Spinal Disorders & Techniques. 16 (4), 418–423
[67] Niosi CA, Zhu QA, Wilson DC, Keynan O, Wilson DR, Oxland TR, 2006. Biomechanical characterization of thethree-dimensional kinematic behaviourof the Dynesys dynamic stabilizationsystem: an in vitro study. European Spine Journal. 15 (6), 913–922
[68] Schilling C, Kru¨ger S, Grupp TM, Duda GN, Blo¨mer W, Rohlmann A, 2011. The effect of design parameters of dynamic pedicle screw systemson kinematics and load bearing: an in vitro study. European Spine Journal. 20 (2), 297-307
[69] Yamamoto I, Panjabi MM, Crisco T, Oxland TOM, 1989. Three-dimensional movements of the whole lumbar spine and lumbosacral joint. Spine. 14 (11), 1256-1260
[70] Zander T, Rohlmann A, Klöckner C, Bergmann G, 2003. Influence of graded facetectomy and laminectomy on spinal biomechanics. European Spine Journal. 12 (4), 427-434
[71] Sharma M, Langrana NA, Rodriguez J, 1995. Role of ligaments and facets in lumbar spinal stability. Spine. 20 (8), 887-900
[72] Panjabi MM, Krag MH, Chung TQ, 1984. Effects of disc injury on mechanical behavior of the human spine. Spine. 9 (7), 707-713
[73] Erbulut DU, Zafarparandeh I, Lazoglu I, Ozer AF, 2014. Application of an asymmetric finite element model of the C2-T1 cervical spine for evaluating the role of soft tissues in stability. Medical Engineering & Physics. 36 (7), 915-921
[74] Lindsey DP, Swanson KE, Fuchs P, Hsu KY, Zucherman JF, Yerby SA, 2003. The effects of an interspinous implant on the kinematics of the instrumented and adjacent levels in the lumbar spine. Spine. 28 (19), 2192-2197
[75] Siddiqui M, Karadimas E, Nicol M, Smith FW, Wardlaw D, 2006. Effects of X-STOP device on sagittal lumbar spine kinematics in spinal stenosis. Journal of spinal disorders & techniques. 19 (5), 328-333
[76] Wilke H-J, Drumm J, Häussler K, Mack C, Steudel W-I, Kettler A, 2008. Biomechanical effect of different lumbar interspinous implants on flexibility and intradiscal pressure. European spine journal. 17 (8), 1049-1056

[77] Hartmann F, Dietz S-O, Hely H, Rommens PM, Gercek E, 2011. Biomechanical effect of different interspinous devices on lumbar spinal range of motion under preload conditions. Archives of orthopaedic and trauma surgery. 131 (7), 917-926
[78] Wiseman CM, Lindsey DP, Fredrick AD, Yerby SA, 2005. The effect of an interspinous process implant on facet loading during extension. Spine. 30 (8), 903-907
[79] Swanson KE, Lindsey DP, Hsu KY, Zucherman JF, Yerby SA, 2003. The effects of an interspinous implant on intervertebral disc pressures. Spine. 28 (1), 26-32
[80] Lafage V, Gangnet N, Sénégas J, Lavaste F, Skalli W, 2007. New interspinous implant evaluation using an in vitro biomechanical study combined with a finite-element analysis. Spine. 32 (16), 1706-1713
[81] Panjabi MM, 2007. Hybrid multidirectional test method to evaluate spinal adjacent-level effects. Clinical Biomechanics. 22 (3), 257-265
[82] Panjabi M, Malcolmson G, Teng E, Tominaga Y, Henderson G, Serhan H, 2007. Hybrid testing of lumbar CHARITE discs versus fusions. Spine. 32 (9), 959-966
[83] Richards JC, Majumdar S, Lindsey DP, Beaupré GS, Yerby SA, 2005. The treatment mechanism of an interspinous process implant for lumbar neurogenic intermittent claudication. Spine. 30 (7), 744-749
[84] Lee J, Hida K, Seki T, Iwasaki Y, Minoru A, 2004. An interspinous process distractor (X STOP) for lumbar spinal stenosis in elderly patients: preliminary experiences in 10 consecutive cases. Journal of spinal disorders & techniques. 17 (1), 72-77
[85] Zucherman JF, Hsu KY, Hartjen CA, Mehalic TF, Implicito DA, Martin MJ, Johnson DR, Skidmore GA, Vessa PP, Dwyer JW, 2005. A multicenter, prospective, randomized trial evaluating the X STOP interspinous process decompression system for the treatment of neurogenic intermittent claudication: two-year follow-up results. Spine. 30 (12), 1351-1358
[86] Miller JD, Miller MC, Lucas MG, 2010. Erosion of the spinous process: a potential cause of interspinous process spacer failure: Report of 2 cases. Journal of Neurosurgery: Spine. 12 (2), 210-213
[87] Bowers C, Amini A, Dailey AT, Schmidt MH, 2010. Dynamic interspinous process stabilization: review of complications associated with the X-Stop device. Neurosurgical focus. 28 (6), E8
[88] Kim DH, Shanti N, Tantorski ME, Shaw JD, Li L, Martha JF, Thomas AJ, Parazin SJ, Rencus TC, Kwon B, 2012. Association between degenerative spondylolisthesis and spinous process fracture after interspinous process spacer surgery. The Spine Journal. 12 (6), 466-472
[89] Shepherd DE, Leahy JC, Mathias KJ, Wilkinson SJ, Hukins DW, 2000. Spinous process strength. Spine. 25 (3), 319-323
[90] Ahn Y-H, Chen W-M, Lee K-Y, Park K-W, Lee S-J, 2008. Comparison of the load-sharing characteristics between pedicle-based dynamic and rigid rod devices. Biomedical Materials. 3 (4), 044101
[91] Ozer AF, Crawford NR, Sasani M, Oktenoglu T, Bozkus H, Kaner T, Aydin S, 2010. Dynamic lumbar pedicle screw-rod stabilization: two-year follow-up and comparison with fusion. The open orthopaedics journal. 4, 137
[92] Bresnahan L, Ogden AT, Natarajan RN, Fessler RG, 2009. A biomechanical evaluation of graded posterior element removal for treatment of lumbar stenosis: comparison of a minimally invasive approach with two standard laminectomy techniques. Spine. 34 (1), 17-23
[93] Abumi K, Panjabi MM, Kramer KM, Duranceau J, Oxland T, Crisco JJ, 1990. Biomechanical evaluation of lumbar spinal stability after graded facetectomies. Spine. 15 (11), 1142-1147
[94] Okawa A, Shinomiya K, Takakuda K, Nakai O, 1996. A cadaveric study on the stability of lumbar segment after partial laminotomy and facetectomy with intact posterior ligaments. Journal of Spinal Disorders & Techniques. 9 (6), 518-526

[95] Yue Z, Gang L, Tongwei C, Jian W, Changqing L, Wenjie Z, Zhengfeng Z, Yong H, Chao Z, 2008. Biomechanical change of lumbar unilateral graded facetectomy and strategies of its microsurgical reconstruction: report of 23 cases. Journal of Medical Colleges of PLA. 23 (2), 98-105

[96] Li H, Wang Z, 2006. Intervertebral disc biomechanical analysis using the finite element modeling based on medical images. Computerized medical imaging and graphics. 30 (6), 363-370

[97] Lee K, Teo E, 2004. Effects of laminectomy and facetectomy on the stability of the lumbar motion segment. Medical engineering & physics 26 (3), 183-192

[98] Ogden AT, Bresnahan L, Smith JS, Natarajan R, Fessler RG, 2009. Biomechanical comparison of traditional and minimally invasive intradural tumor exposures using finite element analysis. Clinical Biomechanics. 24 (2), 143-147

[99] Kiapour A, Ambati D, Hoy RW, Goel VK, 2010. Effect of graded facetectomy on biomechanics of dynesys dynamic stabilization system. Spine. 37 (10), E581-E589

[100] Lehman Jr RA, Kuklo TR, 2003. Use of the anatomic trajectory for thoracic pedicle screw salvage after failure/violation using the straight-forward technique: a biomechanical analysis. Spine. 28 (18), 2072-2077